Original Article

Hesperidin Alleviates Cisplatin-Induced Impairment in Adult Male Albino Rat's Submandibular Gland Through Activation of Secretory Complex Stem Cells (Histological, Immunohistochemical and Biochemical Study)

Ola A. Yahia[1], Samar Asker[1,2,3], Wafaa S. Hamed[1], Nawal Awad Hasanin[1] and Nahla Reda Sarhan[1]

Department of Medical Histology and Cell Biology, Faculty of Medicine, [1]Mansoura University, [2]6th of October University, [3]Delta University, Egypt

ABSTRACT

Introduction: Cisplatin chemotherapy targets many tumors. However, it affects the submandibular gland causing its hypofunction. Hesperidin has antioxidant and anti-inflammatory actions.

Aim of the Work: Was to evaluate the biochemical and histological alterations caused by two regimens of cisplatin application on rat's submandibular gland and to assess the effect of hesperidin against these changes.

Materials and Methods: 70 adult male albino rats were divided into 4 groups. Group I; control rats, Group II was given hesperidin (100mg/kg/day) orally from day 1 until the experiment end. Group III received single high cisplatin dose (intraperitoneally 12mg/kg) on 8th day and subdivided into subgroup IIIa that received cisplatin only and IIIb received cisplatin + hesperidin as group II. Group IV received multiple low cisplatin doses (intraperitoneally 6mg/kg) once a week starting from 8th day and subdivided into subgroup IVa that received cisplatin only and IVb received cisplatin + hesperidin as group II. Submandibular glands were dissected out and processed for biochemical, histological and immunohistochemical studies. c-Kit was used as a stem cell marker.

Results: Subgroups IIIa & IVa showed biochemical, histological, and ultrastructural changes that was more marked in IIIa. There was a significant elevation of malondialdehyde and reduction of antioxidant enzyme activities, disturbance of gland architecture, acinar and duct cell degeneration, significant elevation in % area of collagen fibers and significant reduction in % area of c- kit immune reaction. Subgroups IIIb and IVb showed improvement in the histological picture of the gland with a significant increase in % area of c- kit immune reaction.

Conclusion: Cisplatin causes changes in submandibular gland being more marked with the single high dose. Hesperidin partially alleviates these changes through its antioxidant action and enhanced activation of secretory complex stem cells. So, hesperidin can be used clinically with chemotherapy to prevent its side effects.

Received: 17 November 2022, **Accepted:** 23 December 2022

Key Words: Cisplatin, c-Kit, hesperidin, stem cells, submandibular gland.

Corresponding Author: Nahla Reda Sarhan, PhD, Department of Medical Histology and Cell biology, Faculty of Medicine, Mansoura University, Egypt, **Tel.**: +20 10 0143 8436, **E-mail:** nahlaredasarhan@mans.edu.eg

ISSN: 1110-0559, Vol. 47, No. 1

INTRODUCTION

Cisplatin is an efficient chemotherapy that is commonly used in the therapy of wide variety of malignancies such as head and neck cancers, bladder and lung cancers[1]. It causes crosslinks with DNA purine bases thus interfere with its repair mechanisms, producing injury of DNA with subsequent apoptosis in tumor cells[2]. Despite its potent anti-tumor effect, cisplatin causes oxidative stress leading to severe side effects[3]. Moreover, it worsen the function of the salivary gland and increase the incidence of mucositis[4].

Chemotherapy-induced salivary gland hypofunction can cause numerous sequelae, including xerostomia (dry mouth), which is the most common complication that impair the life quality of the patient. It may cause swallowing problems, speaking difficulties, taste disorder, oral mucositis, and esophageal inflammation[5].

The use of a natural, non-toxic, effective, accessible method of administration compound is needed to prevent xerostomia and oral mucositis following the chemotherapy. Hesperidin is a flavonone glycoside, related to the family of flavonoid, that is present in Citrus species. Flavonoids have analgesic, anti-inflammatory and antioxidant properties[6]. Hesperidin was also reported to have a chemoprotective[7] and radioprotective effects[8].

c-Kit (CD117 or stem cell factor receptor) is a type III transmembrane receptor tyrosine kinase. c-kit is encoded by the protooncogene c-kit that located in the long arm of human chromosome 4. Stem cell factor (SCF) is a c-Kit principal ligand and the interaction between them causes dimerization, autophosphorylation of the activated receptors at tyrosine residues and signal transduction[9]. c-kit-SCF signalling resulting in proliferation, differentiation, inhibition of apoptosis, and chemotaxis in c-kit expressing

 DOI: 10.21608/ejh.2022.172950.1804

cells[10]. c-kit is expressed in several normal cells including different kinds of stem and progenitor cells especially hematopoietic stem cells. In addition, cells of Cajal, germ cells express c-kit[11]. In the submandibular gland, c-kit is a marker of the stem cell population that mainly exist in the ductal cells[12,13].

To our knowledge, no previous research was carried out on the effectiveness of hesperidin against cisplatin-induced submandibular gland damage. However, many studies proved a protective outcome of hesperidin in case of hepatotoxicity[14], nephrotoxicity[15,16] and cardiotoxicity[17].

Therefore, the aim of current work was to evaluate the impact of cisplatin on the submandibular gland of rat by comparing two regimens: the single high and the multiple low dose regimen. In addition, we evaluated the efficacy of hesperidin as an antioxidant to alleviate the cisplatin-induced damage and its ability to restore the glandular stem cells through detection of expression of c-kit a stem cell marker.

MATERIALS AND METHODS

Used materials

Cisplatin a product of Cipla Limited Company, India, available in the form of vials (15663-27-1) containing solution with a concentration of 50 mg/50 ml per bottle.

Hesperidin powder (520-26-3) and phosphate buffered saline (PBS) (7447-40-7) were bought from Sigma Aldrich Company, St. Louis, MO, USA. Hesperidin was dissolved in PBS (200mg Hesperidin in 10ml PBS).

Anti-CD117 (c-Kit) primary antibody (mouse monoclonal antibody, Dako, Carpinteria, California, USA, catalog number R714501F at a dilution 1/100)

Study protocol

An approval for the study protocol was obtained from the institutional review board (IRB) of the faculty of medicine, Mansoura University (MDP.18.02.2). The study was conducted at the house of animal, faculty of pharmacy, Mansoura University. Seventy adult male Sprague Dawley rats 100–120 days old and weighing between 200–250 g were used. The rats were kept in plastic cages under adequate ventilation and temperature on cycles of 12-h light/12-h dark during the experimental period. They were freely provided with water and given the usual rodent chow. Tissue processing and staining were performed at medical histology and cell biology department, laboratory, Mansoura faculty of medicine and E/M units of faculty of science, Alexandria University and Faculty of agriculture, Mansoura university. The study duration was 5 weeks.

Animal grouping

Following an accommodation for 2 weeks, the rats were separated in a random way into 4 groups. all of them were sacrificed 5 weeks from the beginning of the experiment:

Group I (control group) (n=20 rats): this group was subdivided into two subgroups; Ia which received only ordinary diet and water and subgroup Ib that received PBS 5ml\kg/day by orogastric tube (the solvent of Hesperidin).

Group II (Hesperidin group) (n=10 rats): was given hesperidin at a dose of 100mg/kg/day orally by orogastric tube dissolved in PBS[18] from day 1 of the experiment.

Group III (Single high dose cisplatin group) (n=20 rats): was injected intraperitoneally with a single high dose (12mg/kg) of cisplatin at day 8 of the experiment[19]. They were further subdivided into subgroup IIIa (cisplatin only) and subgroup IIIb (cisplatin + hesperidin as in group II).

Group IV (Multiple low doses cisplatin group) (n=20 rats): was injected intraperitoneally with multiple low doses of cisplatin (6mg/kg per week for 4 weeks)[20] starting from day 8 of the experiment. This group were further subdivided into subgroup IVa (cisplatin only) and subgroup IVb (cisplatin + hesperidin as in group II), then sacrificed at the end of 5 weeks and 24 hours after the last dose of cisplatin injection.

Sample obtaining and preparation

At the date of sacrifice, anesthesia was done for the animals using intraperitoneal injection of sodium pentobarbital (40 mg/kg body weight)[21]. For electron microscopy samples, some animals from each group underwent perfusion with 0.1 M sodium phosphate buffer including 2.5% glutaraldehyde in their left ventricles. Both submandibular glands were carefully dissected out, rinsed by saline and processed for biochemical, histological and immunohistochemical studies.

Biochemical study

Specimens from the left submandibular gland were rinsed using a solution of phosphate buffered saline (pH 7.4) containing heparin for clot and RBCs elimination. After that, homogenization of the tissues was done in 7 ml cold potassium phosphate buffer per gram tissue and centrifugation occur at 4000 revolutions/ minute for 15 minutes at 4°C. The supernatant liquid was collected and applied for the undermentioned assays:

Assay of Lipid peroxidation

Colorimetric assessment of lipid peroxidation was performed through measurement of the level of malondialdehyde (MDA) that expressed as nmol/ml. The method of measurement was recorded by Tukozkan *et al*.[22] using thiobarbituric acid (TBA) reaction. The kit was purchased from the company of Bio-Diagnostics (Dokki, Giza, Egypt, catalog number. MD 2529).

Assay of Antioxidant enzymes activity

The activities of superoxide dismutase (SOD) and Catalase (CAT) enzymes were measured using Leite *et al*.[23] and Aebi[24] methods and expressed as U/ml and U/L respectively. The enzyme Activities were estimated calorimetrically using the commercial kits

(Bio-Diagnostics; Dokki, Giza, Egypt, catalog number; SD 2521 For SOD, CA 2517) for CAT.

Histological study

A- Light microscopic study

Small specimens from the right submandibular glands underwent fixation by 10% buffered formalin for one day, dehydration in ascending alcohol concentrations, clearance by xylene then embedding in paraffin wax. 5 µm thick paraffin sections were cut and stained with:

Hematoxylin and Eosin (H&E) stain for routine histological examination[25]

Mallory's Trichrome stain for demonstration of collagenous fibers[26].

Immunohistochemical staining: Anti- CD 117(c-Kit) antibody was used as a distinctive marker for identification of glandular stem cells[27,28]. The staining procedure was used according to Sanderson *et al*.[29]. The deparaffinized gland sections were processed and incubated with primary anti CD-117 antibody for 1 hour (dilution 1/100). Negative controls were prepared from submandibular gland with the same technique after omitting the primary antibody. Human GIT stromal tumor was used as a positive control. Positive reaction was considered when there was brown cytoplasmic staining.

B- Electron microscopic study[30]

Tiny specimens from the right submandibular glands underwent fixation at 4°c overnight in the refrigerator by using 2% paraformaldehyde and 2.5% buffered glutaraldehyde and post fixation for 1 hour in 1% osmic acid. After the usual processing, semithin and ultrathin sections (60–80 nm) were cut. The latter were stained with uranyl acetate and lead citrate and examined by JEOL-JEM-100 SX transmission electron microscope.

Morphometric and statistical analysis

Quantitative assessment was done for some parameters including the number and diameter of granular convoluted tubules (GCTs) / high power field (HPF) in H&E-stained sections. The diameter of GCT was done by measuring more than one diameter from 5 random GCTs in the field[31] and the largest diameter was taken from each tubule because of the irregularity in the tubule shape. Percentage area % of collagen fibers in Mallory's trichrome stained sections and Percentage % area of c-kit immune reaction was also measured. For assessment, 5 slides from each specimen were examined. In each slide 5 non-overlapping microscopic fields of the submandibular gland were analysed. Photos from the slides was captured using x40 objective lens by a digital camera (E420, China) settled on an Olympus microscope with 0.5x photo adaptor. Photo analyses were carried out by VideoTesT Morphology software (VideoTesT, Russia, Saint-Petersburg).

The data was analyzed using Statistical Package for Social Science software computer program version 26 (SPSS, Inc., Chicago, IL, USA). Shapiro-Wilk was used to test normality of data. Quantitative data was presented in the form of mean ± standard deviation (SD). To determine the significance of changes through the variable study groups; we used One Way Anal¬ysis of Variance (ANOVA) test. Post-hoc Tukey test was used following ANOVA to compare the quantitative means of more than two variable groups. Statistical significance was considered when $P\ value \leq 0.05$[32].

RESULTS

N.B two rats from subgroup IIIa died and couldn't survive until the end of the study.

Biochemical results

The MDA level of subgroups IIIa and IVa revealed significant elevation ($P \leq 0.05$) compared to the control group I, group II, and subgroups III b and IVb respectively. However, MDA level in subgroup IVa showed a significant reduction relative to subgroup IIIa (Histogram.1). The SOD and CAT activities of subgroup III and IVa showed significant ($P \leq 0.05$) reduction than group I, II and subgroups III b and IVb respectively. However, the enzyme activities showed significant elevation in subgroup IVa compared to III a (Histogram. 2).

Light microscopic results

H&E results

Group I (control group) & **group II** (Hesperidin treated group): Sections from both groups similarly revealed the characteristic histological structure of rat submandibular gland and statistically there was insignificant difference between them. The gland was covered by thin capsule and divided by thin septa into lobes and lobules. Variable shaped atypical serous acini and the ducts were present iside the lobules forming the secretory complex. Myoepithelial cells were found around the acini and ducts (Figures 1A,B). The cells of the acini were pyramidal with basophilic cytoplasm and rounded basal nuclei. The lining cells of the intercalated duct was cuboidal cells. The lining of the striated duct was high cubical cells with basal eosinophilic striations (Figure 1C). The cell lining of GCTs was columnar and had numerous eosinophilic granules (Figure 1D). The interlobular duct was lined with simple columnar to pseudostratified columnar epithelium (Figure 1B).

Subgroups IIIa (single high dose cisplatin treated rats) and IIIb (single high dose cisplatin + hesperidin treated rats): Sections from submandibular glands of subgroup IIIa displayed marked histological changes. There was noticeable capsule thickening with dilated congested blood vessels and inflammatory cell infiltration. The acinar cells showed cytoplasmic vacuolations (Figures 2A,B). The Striated ducts showed dilatation with stagnant vacuolated secretion, cytoplasmic vacuolations and many pyknotic nuclei (Figures 2B,C). Degenerated GCTs with marked destruction of their lining cells and loss of secretory

granules were observed and the nuclei were pyknotic or karyolitic. cells (Figure 2D). The interlobular ducts appeared dilatated with stagnant vacuolated secretion (Figure 2E). According to statistical analysis, the number and diameter of GCTs/HPF of this subgroup showed significant ($P \leq 0.05$) reduction compared to control group I and group II (Histogram 3).

On the other hand, subgroup IIIb showed much better histological picture compared to subgroup IIIa. Thin capsule and preserved structure of acini, GCTs were seen. However, some structural changes were present in the form of cytoplasmic vacuolations, nuclear pyknosis in GCTs lining cells (Figures 2F,G). The striated ducts showed intact structure and vesicular nuclei but there were empty cytoplasmic areas (Figure 2H). The number and diameter of GCTs/HPF were significantly ($P \leq 0.05$) higher than subgroup IIIa (Histogram 3).

Subgroups IVa (Multiple low dose cisplatin treated rats) and IVb (Multiple low dose cisplatin + hesperidin treated rats): Sections from submandibular glands of Subgroup IVa showed thick septa containing dilated congested blood vessels. The acinar cells had ill-defined boundaries and showed cytoplasmic vacuolations (Figure 3A). Dilated interlobular ducts and dilated striated duct with stagnant secretion and Lost basal striation were also found (Figures 3 A,B). The GCTs showed few or lost granules and pyknotic nuclei in some lining cells. (Figure 3C). The number and diameter of GCTs/HPF revealed significant ($P \leq 0.05$) reduction relative to the control group I and group II. However, these parameters were significantly higher than subgroup III a (Histogram.3).

Subgroup IVb showed less histological alterations compared to subgroup IVa. The capsule and septa were thin. The acini, striated ducts and GCTs relatively restored their structure (Figures 3 D,E,F). Although, some vacuolated acinar cells (Figure 3D) and some pyknotic or karyolitic nuclei in GCTs were still found (Figure 3F). The number and diameter of GCTs/HPF of this group was significantly higher than subgroup IVa (Histogram 3).

Mallory's trichrome results

Group I and group II: Demonstrated no difference between them. The gland demonstrated few regular collagen fibers in the thin capsule, in thin interlobular septa, around the acini and ducts (Figures 4A,B).

Subgroups IIIa and IIIb: Subgroup IIIa showed noticeable increase in irregular collagen fibers in the thick capsule (Figure 5A), in the thick septa, around the acini, periductal and peri-acinar (Figure 5B). The percentage area of collagen fibers showed significant ($P \leq 0.05$) elevation compared to the control group I and group II (Histogram 4). However, subgroup IIIb showed fewer regular collagen fibers at the same areas (Figures 5 C,D) and the percentage area of the collagen fibers showed significant ($P \leq 0.05$) reduction relative to subgroup IIIa (Histogram 4).

Subgroups IVa and IVb: Subgroup IVa showed many irregular collagen fibers in the thick capsule (Figure 6A), in the septa, Peri acinar and periductal (Figure 6B). The percentage area of the collagen fibers in this group exhibited a significant ($P \leq 0.05$) increase compared to control group I and group II. However, it showed significant decrease relative to subgroup IIIa (Histogram 4). On the other hand, subgroup IVb showed fewer regular collagen fibers at the same regions (Figures 6 C,D) and the percentage area of the collagen fibers showed significant ($P \leq 0.05$) reduction compared to subgroup IVa (Histogram 4).

Immunohistochemical results

Group I and group II: Immunohistochemically stained sections for c-Kit in the control group I and group II showed similar pattern of immune reaction. A strong positive cytoplasmic reaction was noted in many cells of the intercalated duct, striated duct, interlobular duct (Figures 7 A-C) and in the myoepithelium (Figure 7D).

Subgroups IIIa and IIIb: Subgroup IIIa showed faint c-Kit immunoreaction in the ducts except for few cells in the striated and intercalated ducts and in the myoepithelium (Figures 8 A-C). However, subgroup IIIb showed strong reaction in the cells of ducts and myoepithelium (Figure 8 D-F). The percentage area of c-kit immune reaction in subgroup IIIa was significantly ($P \leq 0.05$) lower than control group I and group II and it was significantly higher in subgroup IIIb than subgroup IIIa (Histogram. 5).

Subgroups IVa and IVb: Subgroup IVa showed positive c-kit immunoreactivity in some cells of the striated and intercalated ducts and in the myoepithelial cells (Figures 9 A-C). On the other hand, subgroup IVb showed abundant reaction in more ductal and myoepithelial cells (Figure 9 D-F). The percentage area of c-kit immune reaction in subgroup IVa was significantly lower than control group I and group II. However, it was significantly higher than subgroup IIIa and it was significantly higher in subgroup IVb than subgroup IVa (Histogram. 5).

Electron microscopic results

Control group I & group II: The submandibular gland of both groups revealed similar ultrastructure. The acinar cells appeared with different secretion stages either with numerous apical moderate electron dense, electron lucent or no granules. The usual cell organelles and rounded euchromatic nuclei were also found in the acinar cells (Figures 10 A,B). The GCT cells showed apical electron dense granules, euchromatic nucleus, numerous mitochondria and lateral interdigitations between the adjacent cells (Figure 10C). The striated duct was lined with Light & dark cells that had euchromatic nuclei and many mitochondria (Figure 10D). The cells' apical part showed tight junction, desmosomes, lateral interdigitations and moderate electron dense granules (Figure 10E) while the basal part showed basal infoldings with elongated mitochondria aligned in between (Figure 10F).

Subgroups IIIa and IIIb: Subgroup IIIa revealed evident ultrastructural changes in the form of small secretory granules or merged ones with condensed content, pyknotic nuclei and dilated rER cisternae in the cells of acini (Figure 11A). The GCT cells showed nuclei with corrugated nuclear membrane and wide perinuclear space, swollen degenerated mitochondria with matrix electron dense material, dilated Golgi, multiple vacuoles, and rarefied cytoplasm (Figure 11B). The striated duct showed disrupted luminal border, separation and loss of cellular junctions, heterochromatic nuclei with irregular nuclear membrane and wide perinuclear space, dilated Golgi, swollen mitochondria, lysosomes, rarefied cytoplasm, and loss of basal infoldings (Figures 11C,D).

On the other hand, subgroup IIIb showed better ultrastructure. The acinar (Figure 12A) and GCT cells (Figure 12B) showed numerous apical granules, intact rER and mitochondria. Heterochromatic nuclei and dilated Golgi were still observed. In addition, the striated duct cells showed intact apical border and cell junctions and intact mitochondria (Figure 12C). There was restoration of basal infoldings but with irregular mitochondrial arrangement. Shrunken heterochromatic nuclei and secondary lysosomes were noted (Figure 12D).

Subgroups IVa and IVb: Subgroup IVa displayed some ultrastructural alterations including acinar cells with heterochromatic nuclei and irregular nuclear membrane, fragmented rER, and vacuoles (Figure 13A). The GCT cells also showed heterochromatic nuclei with irregular nuclear membranes and wide perinuclear space, dilated Golgi, multiple vacuoles, autophagosomes, and areas of rarefied cytoplasm (Figure 13B). The cells of striated duct showed irregularity and disruption of desmosomes, mitochondrial swelling with cristolysis. Dilated Golgi, lysosomes, areas of rarefied cytoplasm and lost basal infoldings (Figures 13 C,D). However, Subgroup IVb showed marked improvement in the ultrastructure relative to subgroup IVa in the acinar (Figure 14A) and lining cells of GCT (Figure 14B) and striated ducts (Figures 14 C,D). However, there was still some heterochromatic nuclei in the acinar and GCT cells (Figures 14A,B) and irregular mitochondrial arrangement in between the restored basal infoldings in the striated ducts (Figure 14D).

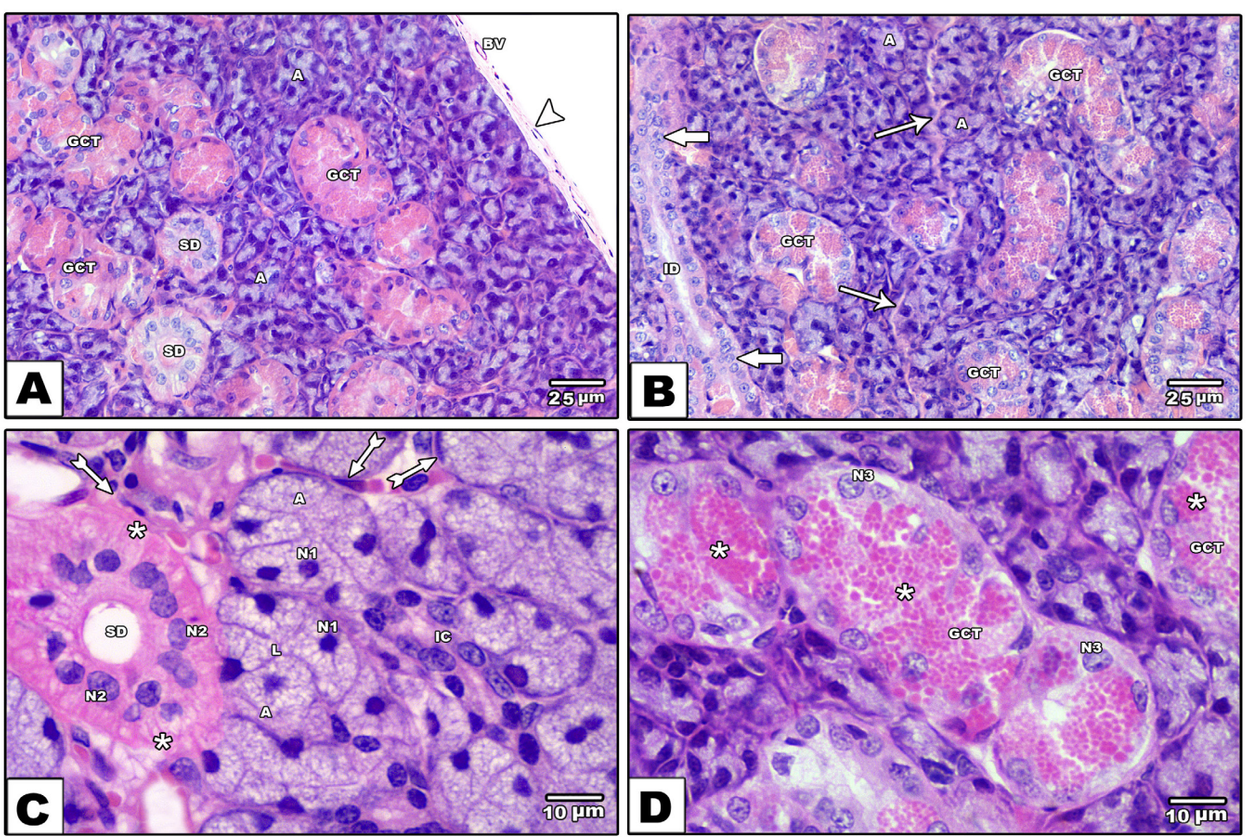

Fig. 1: Tissue sections in the rat submandibular gland of Group I (control group). A&B: showing thin capsule covers the gland (arrowhead) containing blood vessels (BV) and septa (arrows) divides the gland into lobes and lobules. Variable shaped secretory acini (A) and different types of ducts are seen; the striated ducts (SD), the granular convoluted tubules (GCTs) and the larger excretory (interlobular) ducts (ID) that are lined with simple to pseudo stratified columnar epithelium (thick arrows). C: The acini (A) are lined with serous pyramidal cells having broad base and narrow apex abutting a central narrow lumen (L) and shows basophilic cytoplasm and rounded basal nuclei (N1). The Intercalated duct (IC) is seen lined with simple cuboidal epithelial cells. The SD is lined by high cubical cells having rounded nuclei (N2) and basal eosinophilic basal striations (*). Myoepithelial cells (tailed arrows) are observed surrounding the acini and the ducts D: The GCTs are lined with columnar cells with numerous characteristic eosinophilic cytoplasmic granules (*) and open face nuclei (N3) (H&E; A&B x 400, C&D x 1000).

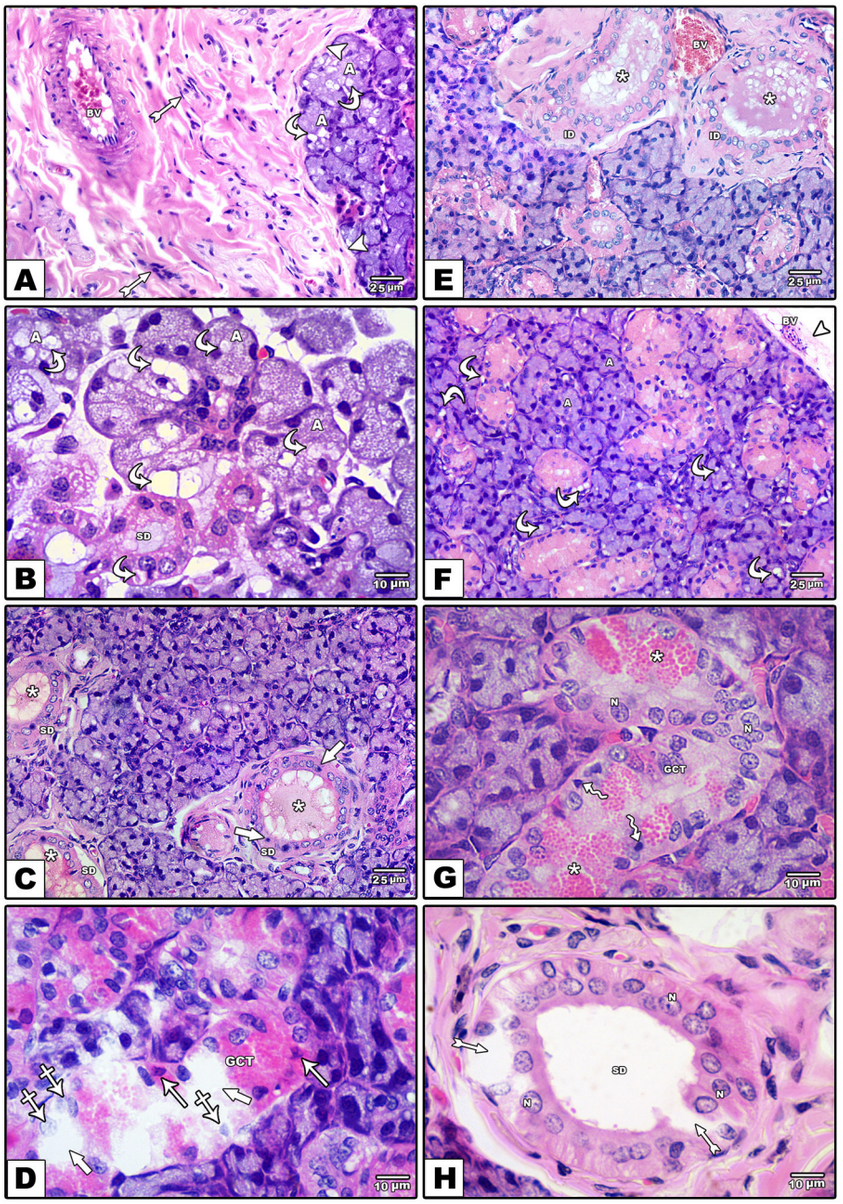

Fig. 2: Tissue sections in the rat submandibular gland of subgroups IIIa (A-E) & IIIb (F-H). A: showing marked thickening of the capsule (arrow heads) that contain dilated, thickened, congested blood vessel (BV) and inflammatory cell infiltration (tailed arrows). Vacuolated acinar cells were noticed (curved arrows). B: showing cytoplasmic vacuolations (curved arrows) in the cells lining the acini (A) and striated ducts (SD). C: the striated ducts (SD) appear dilated with stagnant vacuolated secretion (*). The nuclei in many lining cells are pyknotic (thick arrows). D: showing a degenerated granular convoluted tubule (GCT) with marked destruction of its lining cells leaving large empty spaces with loss of granules (thick arrows). Some nuclei are pyknotic (arrows) while others show karyolysis (crossed arrows). E: The interlobular ducts (ID) are dilated with stagnant vacuolated secretions (*). Note the congested dilated blood vessel (BV). F: showing thin capsule (arrowhead) with congested blood vessel (BV) and preserved acinar (A) structure however, some acinar and GCT cells are vacuolated (curved arrows). G: The GCTs show preserved structure with the characteristic eosinophilic granules (*) and vesicular nuclei (N), however, some nuclei show pyknosis (zigzag arrows). H: The striated ducts (SD) lining cells exhibited vesicular nuclei (N). Empty cytoplasmic areas (tailed arrows) in some cells are observed (H&E; A, C, E & F x400, B, D, G & H x 1000)

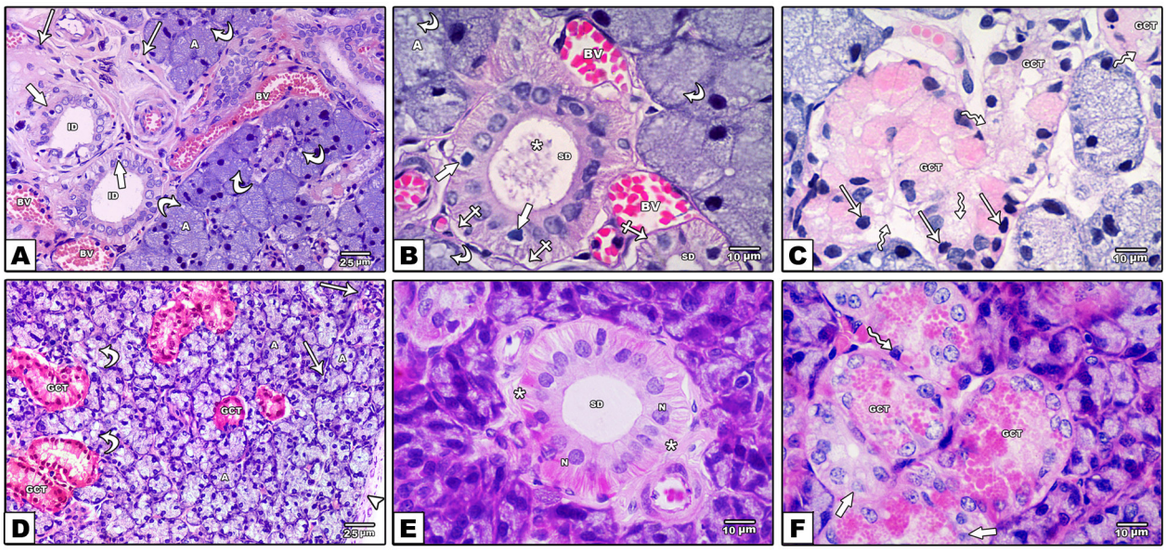

Fig. 3: Tissue sections in the rat submandibular gland of subgroup IVa (A-C) & IVb (D-F). A&B: showing thick septa (arrows) between the gland lobules. Dilated congested blood vessels (BV) are seen in the septa and inside the lobules. The lining cells of the acini (A) appear with ill-defined boundaries and show cytoplasmic vacuolations (curved arrows). Dilated interlobular ducts (ID) and dilated striated duct (SD) with stagnant secretion (*) and Loss of basal striation are seen (crossed arrows}. Some intraepithelial lymphocytes (thick arrows) are detected between the duct cells. C: showing granular convoluted tubules (GCT) with few or lost secretory granules (zigzag arrows) and pyknotic nuclei (arrows). D: a relatively thin capsule (arrowhead) and septa (arrows) and intact secretory acini (A) are found. Some acinar cells show vacuolated cytoplasm (curved arrows). GCTs were seen. E: showing intact striated duct (SD) with vesicular nuclei (N) and basal eosinophilic striations (*). F: The GCT demonstrated the eosinophilic cytoplasmic granules, however, some nuclei appear pyknotic (zigzag arrow) or karyolitic (thick arrows). (H&E; A & D x400, B, C, E & F x 1000)

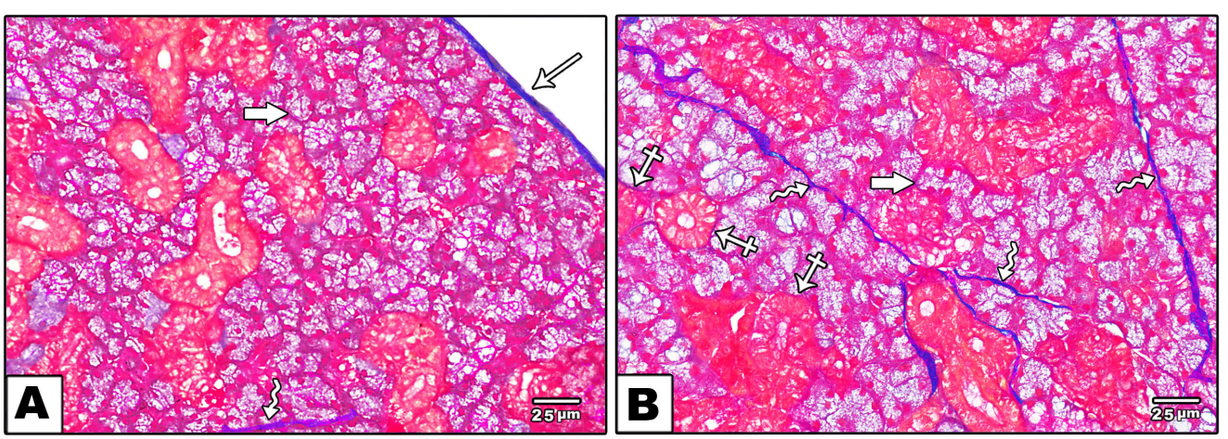

Fig. 4: Tissue sections in the rat submandibular gland of Group I. A&B: showing few regular blue stained collagenous fibers in the thin fibrous capsule (arrow), in the thin interlobular septa (zigzag arrows) and around the acini (thick arrows) and the ducts (crossed arrows) (Mallory's trichrome X 400)

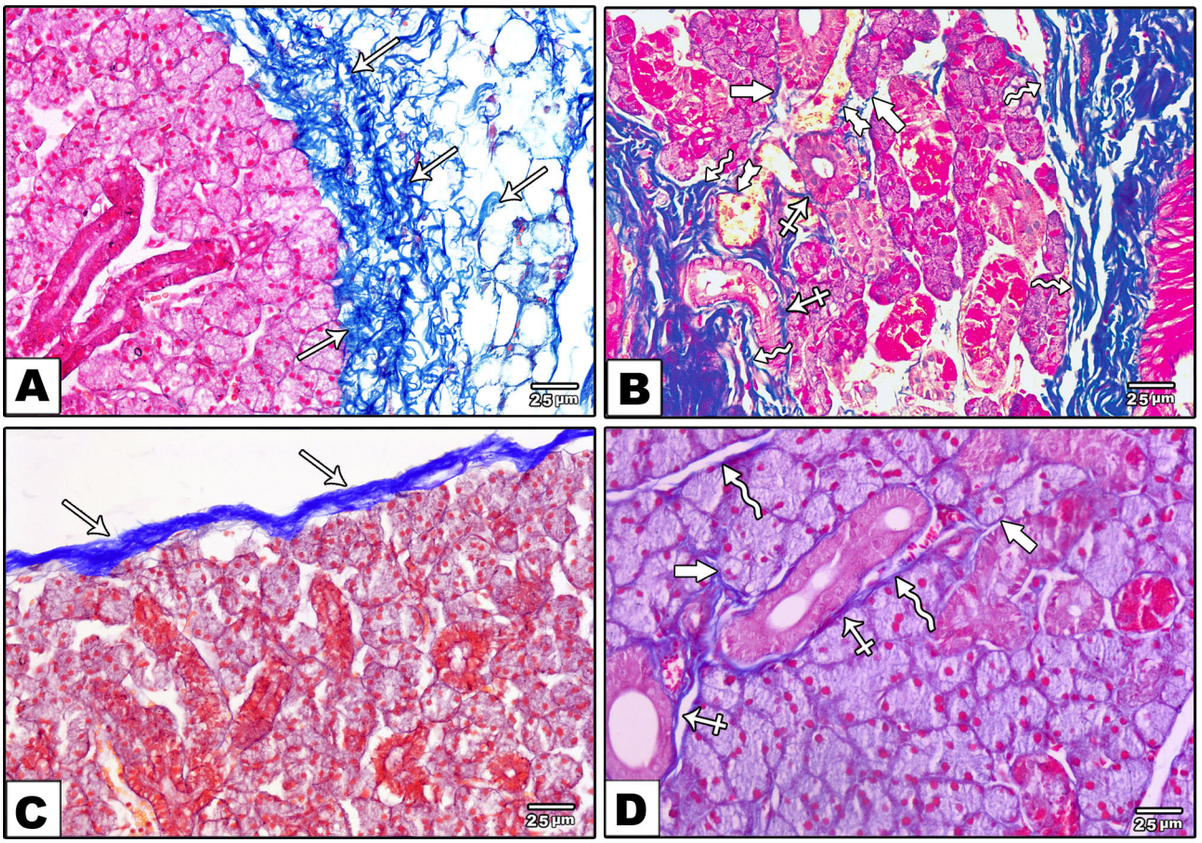

Fig. 5: Tissue sections in the rat submandibular gland of subgroups IIIa (A & B) and IIIb (C&D). A: showing excessive accumulation of irregular collagenous fibers in the thickened capsule (arrows). B: excessive irregular collagen fibers was seen in the thickened trabeculae (zigzag arrows) and around the acini (thick arrows), the ducts (crossed arrows) and the blood vessels (tailed arrows). C: showing few regular collagenous fibers in the relatively thin capsule (arrows). D: few regular collagenous fibers in the thin interlobular septa (zigzag arrows), around the acini (thick arrows) and the ducts (crossed arrows) was noted (Mallory's trichrome X 400)

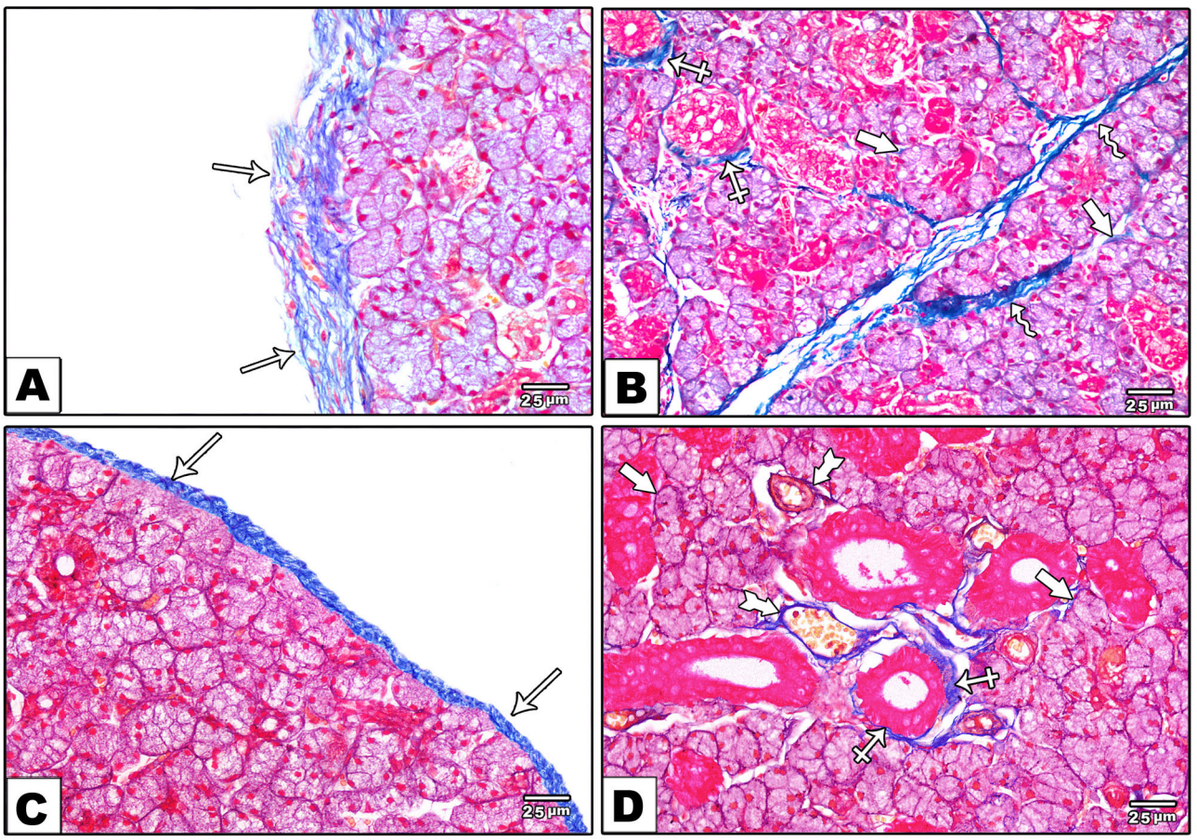

Fig. 6: Tissue sections in the rat submandibular gland of subgroups IVa (A & B) and IVb (C&D). A: showing excessive irregular collagenous fibers in the thick capsule (arrows). B: showing abundant irregular collagen fibers in the interlobular septa (zigzag arrows) and around the acini (thick arrows) and the ducts (crossed arrows). C: showing some regular collagenous fibers in the capsule (arrows). D: Some regular collagenous fibers is observed around the acini (thick arrows), the ducts (crossed arrows) and congested blood vessels (tailed arrows) (Mallory's trichrome X400)

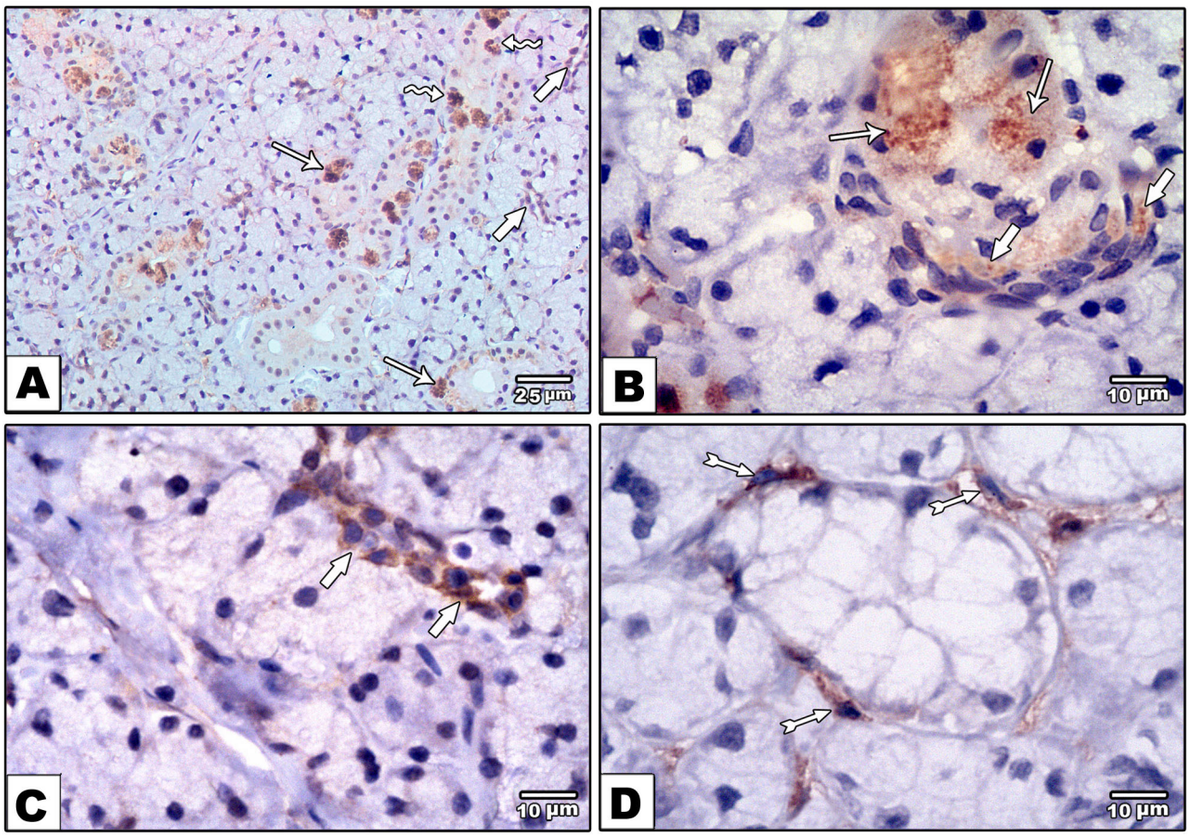

Fig. 7: c-Kit immunoreaction in the rat submandibular gland of Group I. A-C: showing strong positive cytoplasmic immune reaction in many cells of the striated ducts (arrows), the intercalated ducts (thick arrows), interlobular duct (zigzag arrows). D: Strong positive cytoplasmic c-Kit reaction is seen in the myoepithelial cells (tailed arrows) (c-kit immunostaining; A x 400, B-D x1000).

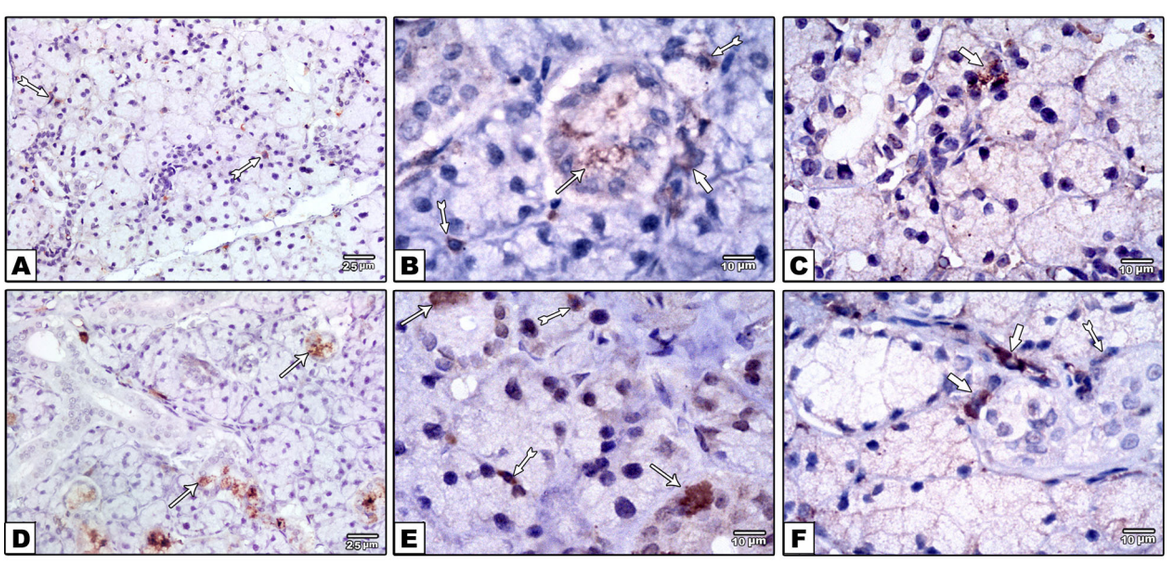

Fig. 8: c-Kit immunoreaction in the rat submandibular gland of Subgroups IIIa (A-C) and IIIb (D-F). A-C: showing faint immune reaction in the ducts. The reaction appears in few cells of the striated duct (arrow), the intercalated ducts (thick arrows) and in the myoepithelial cells (tailed arrows). D-F: showing strong immune reaction in the cells of the striated ducts (arrows), intercalated ducts (thick arrows) and in the myoepithelial cells (tailed arrows) (c-kit immunostaining; A&D x 400, B, C, E&F x1000)

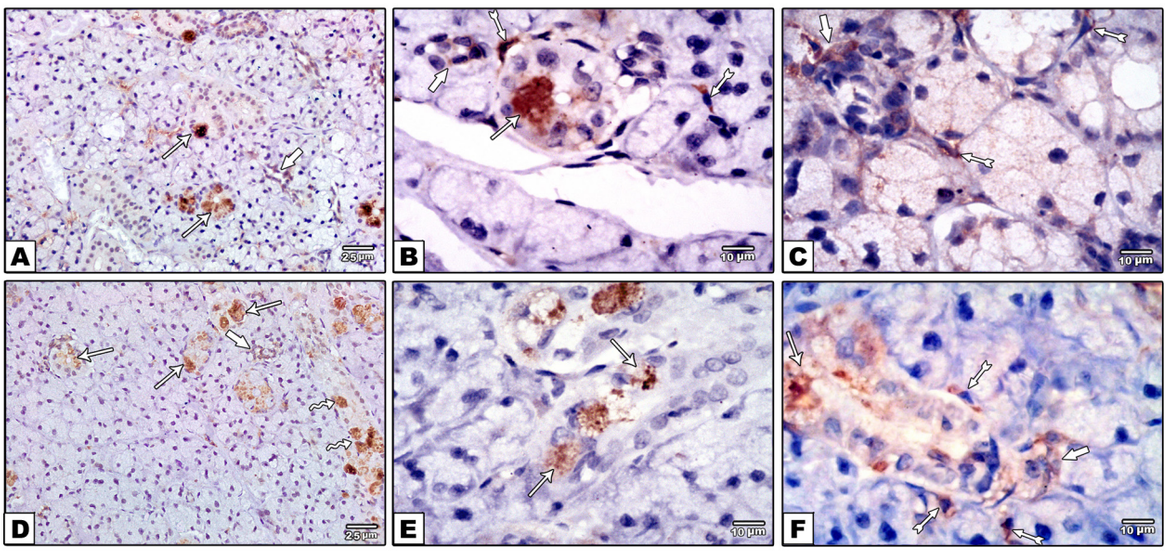

Fig. 9: c-Kit immunoreaction in the rat submandibular gland of Subgroups IVa (A-C) and IVb (D-F). A-C: showing positive c-kit immune reaction in some cells of the striated ducts (arrows), the intercalated ducts (thick arrows) and in the myoepithelial cells (tailed arrows). D-F: showing abundant immune reaction in more cells in the striated ducts (arrows), intercalated ducts (thick arrows), the interlobular ducts (zigzag arrows) and in the myoepithelial cells (tailed arrows) (c-kit immunostaining; A&D x 400, B, C, E&F x1000)

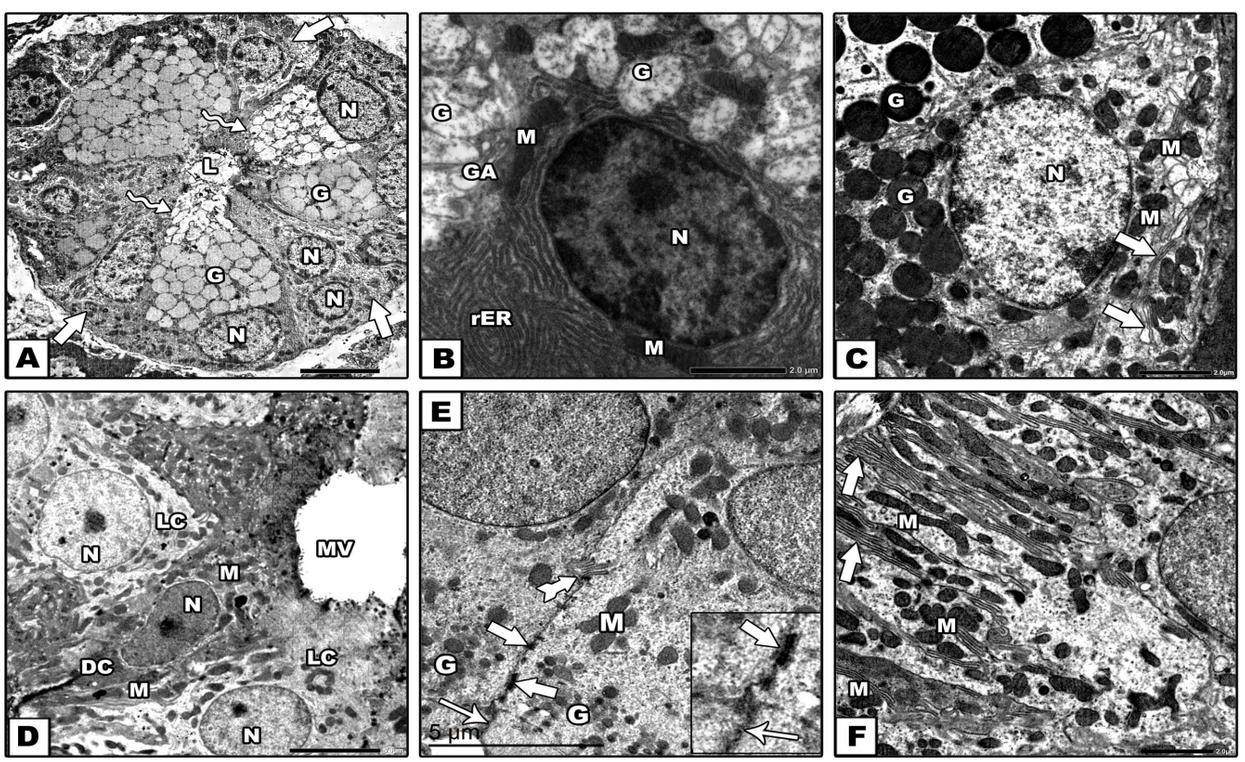

Fig. 10: Electron micrographs of the rat submandibular gland of Group I. A: showing an acinus and their lining cells surrounding a central lumen (L). The acinar cells appear with variable stages of secretion. Some contain numerous apical moderate electron dense secretory granules (G) or electron lucent granules (zigzag arrows) or others show no granules (thick arrows). Rounded euchromatic nuclei (N) are also shown in the acinar cells. B: showing an acinar cell with euchromatic nucleus (N), rough endoplasmic reticulum cisternae (rER), supranuclear Golgi complex (GA) and mitochondria (M). C: showing GCT lining cell contains apical electron dense granules (G), rounded euchromatic nucleus (N), numerous mitochondria (M) and lateral interdigitations between the neighboring cells (thick arrows). D-F: showing the striated duct. D; It lines with light (LC) & dark cells (DC). They have euchromatic nuclei (N) and many mitochondria (M). Microvilli (MV) are projecting from the apical border of the cells. E; The apical part of cells shows tight junction (arrow), desmosomes (thick arrows), lateral interdigitations (tailed arrow), moderate electron dense granules (G) and mitochondria (M). F; The basal part of the cells shows basal infoldings (thick arrows) with elongated mitochondria (M) aligned in between the folds (Uranyl acetate & lead citrate; A x 1000, B, C&F x 4000, D &E x1500, Inset X3000)

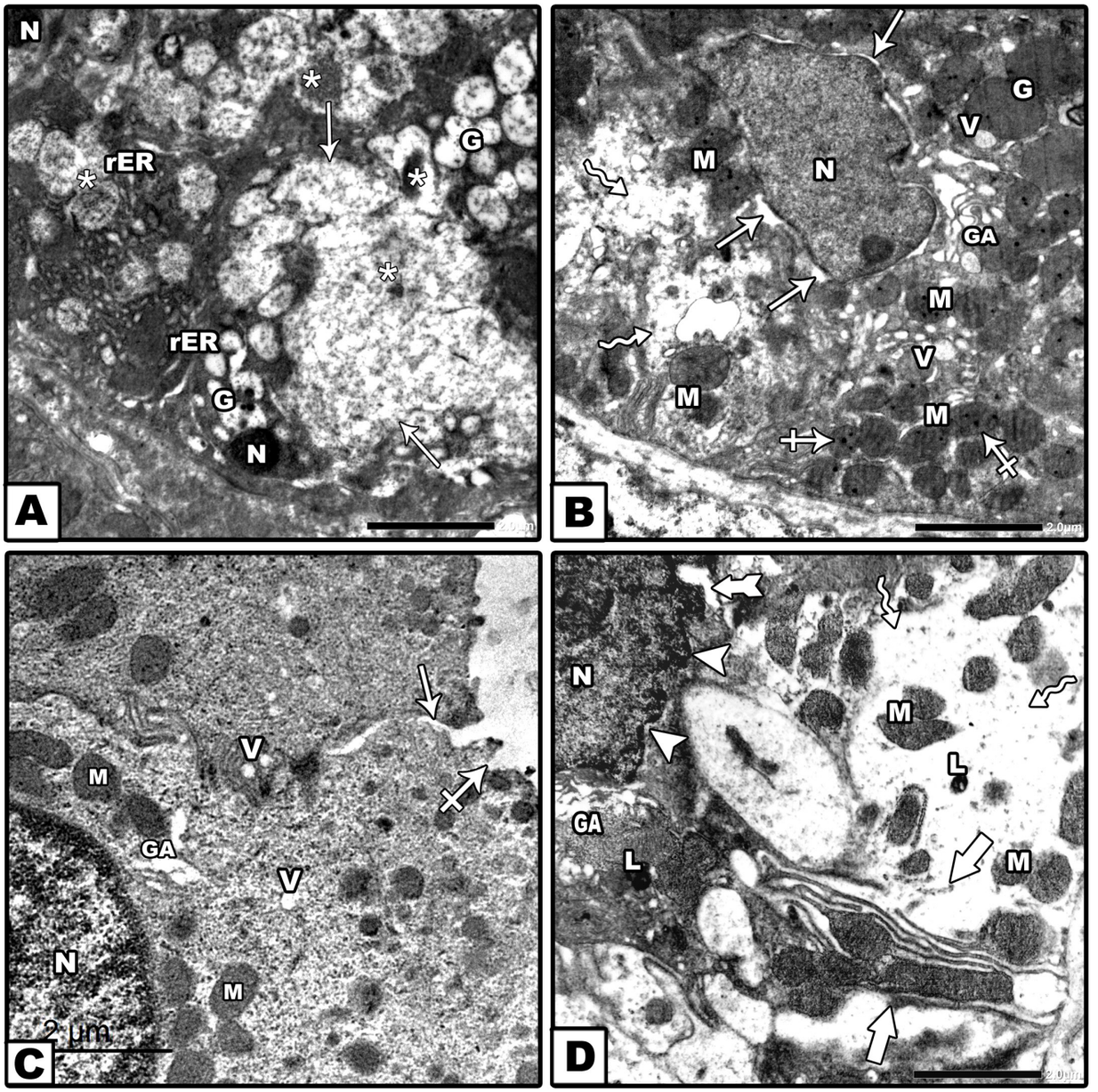

Fig. 11: Electron micrographs of the rat submandibular gland of Subgroup IIIa. A: The acinar cells show small secretory granules (G) or merged ones (arrows). They contain condensed contents (*). Pyknotic nuclei (N) and dilated cisternae of rER are observed (rER). B: The cell of GCT shows a nucleus (N) with corrugated nuclear membrane and wide perinuclear space (arrows), swollen degenerated mitochondria (M) with electron dense material in the matrix (crossed arrows), dilated Golgi (GA), multiple vacuoles (V) and rarefied cytoplasm (zigzag arrows). Some apical moderate electron dense secretory granules are also detected (G). C & D: showing the striated duct with disrupted luminal border (crossed arrow), separation and loss of junctions between the cells (arrow). The nuclei are heterochromatic (N). Some shows irregular nuclear membrane (arrow heads) and wide perinuclear space (tailed arrow). Cytoplasmic vacuoles (V) , areas of rarefaction (zigzag arrows), Dilated Golgi (GA), swollen mitochondria (M) and lysosomes (L) are noticed. There is also loss of basal infoldings (thick arrows) (Uranyl acetate and lead citrate; A, B &D x 4000, Cx2000).

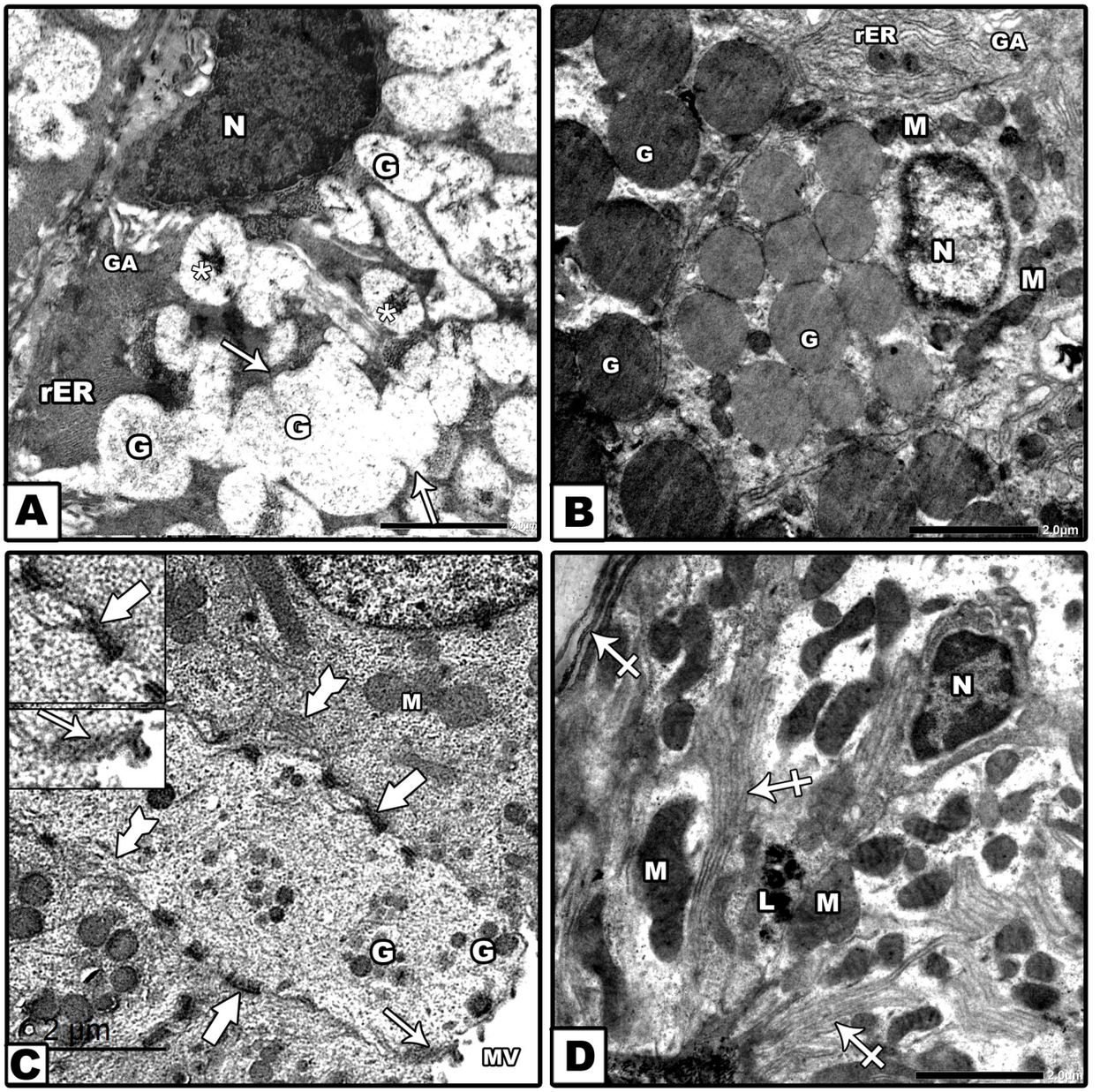

Fig. 12: Electron micrographs of the rat submandibular gland of Subgroup IIIb . A: The acinar cell shows numerous apical electron lucent secretory granules (G), some of them are merged (arrows) while others contain electron dense material (*). Packed parallel rER cisternae (rER), heterochromatic nucleus (N) and dilated Golgi saccules (GA) are observed. B: The GCT cells show secretory granules (G) of variable electron densities, rER cisternae (rER) and many mitochondria (M). However, shrunken nucleus (N) with peripheral chromatin and dilated Golgi saccules (GA) are detected. C: shows striated duct with intact apical border and microvilli (MV), intact tight junction (arrows), desmosomes (thick arrows) and lateral interdigitations (tailed arrows) between the cells. Some electron dense granules (G) and mitochondria (M) are detected. D: The basal part of the striated duct shows restoration of the infoldings (crossed arrows) with irregular mitochondrial arrangement (M), shrunken heterochromatic nucleus (N). and secondary lysosomes (L) (Uranyl acetate and lead citrate; A, B&D x 4000, C x2000, Inset x3000.

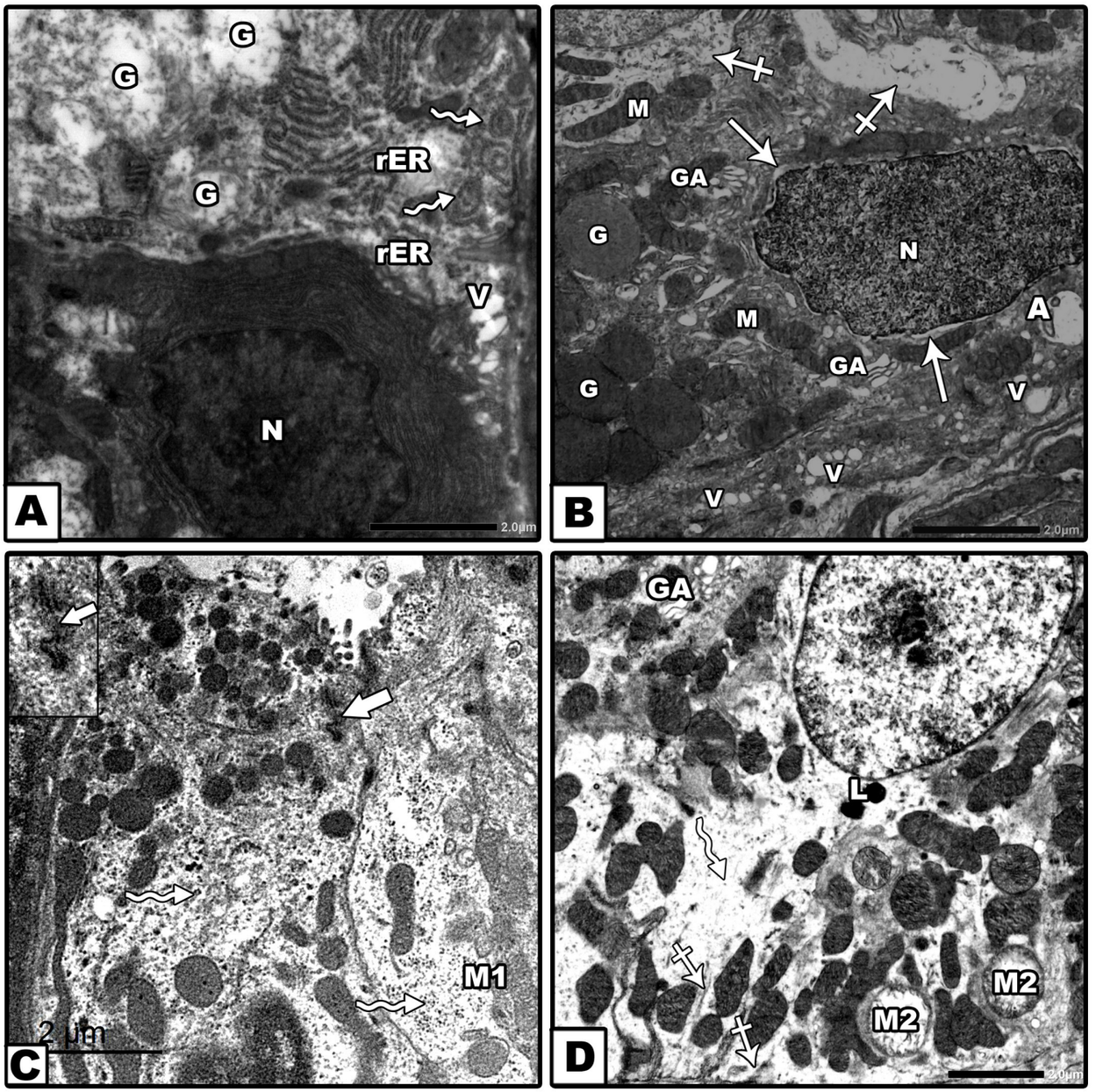

Fig. 13: Electron micrographs of the submandibular gland of Subgroup IVa. A: shows an acinar cell with electron lucent granules (G) and heterochromatic nucleus (N) with irregular nuclear membrane. Fragmented rER, many polyribosomes (zigzag arrows) and vacuoles (V) are also noticed. B: showing a GCT lining cell. There is a nucleus (N) with irregular nuclear membrane and wide perinuclear space (arrows), dilated Golgi (GA), multiple vacuolations (V), autophagosomes (A) and areas of rarefied cytoplasm (crossed arrows). Electron dense granules (G) and mitochondria (M) are seen. C&D: show the striated duct. There is irregularity and disruption of desmosomes between the cells (thick arrows). Some mitochondria are distorted (M1) or swollen with cristolysis (M2). Dilated Golgi (GA), lysosomes (L), areas of rarefied cytoplasm (zigzag arrows) and lost basal infoldings (crossed arrows) are observed (Uranyl acetate & lead citrate; A, B&D X4000; CX 2000, Inset X3000).

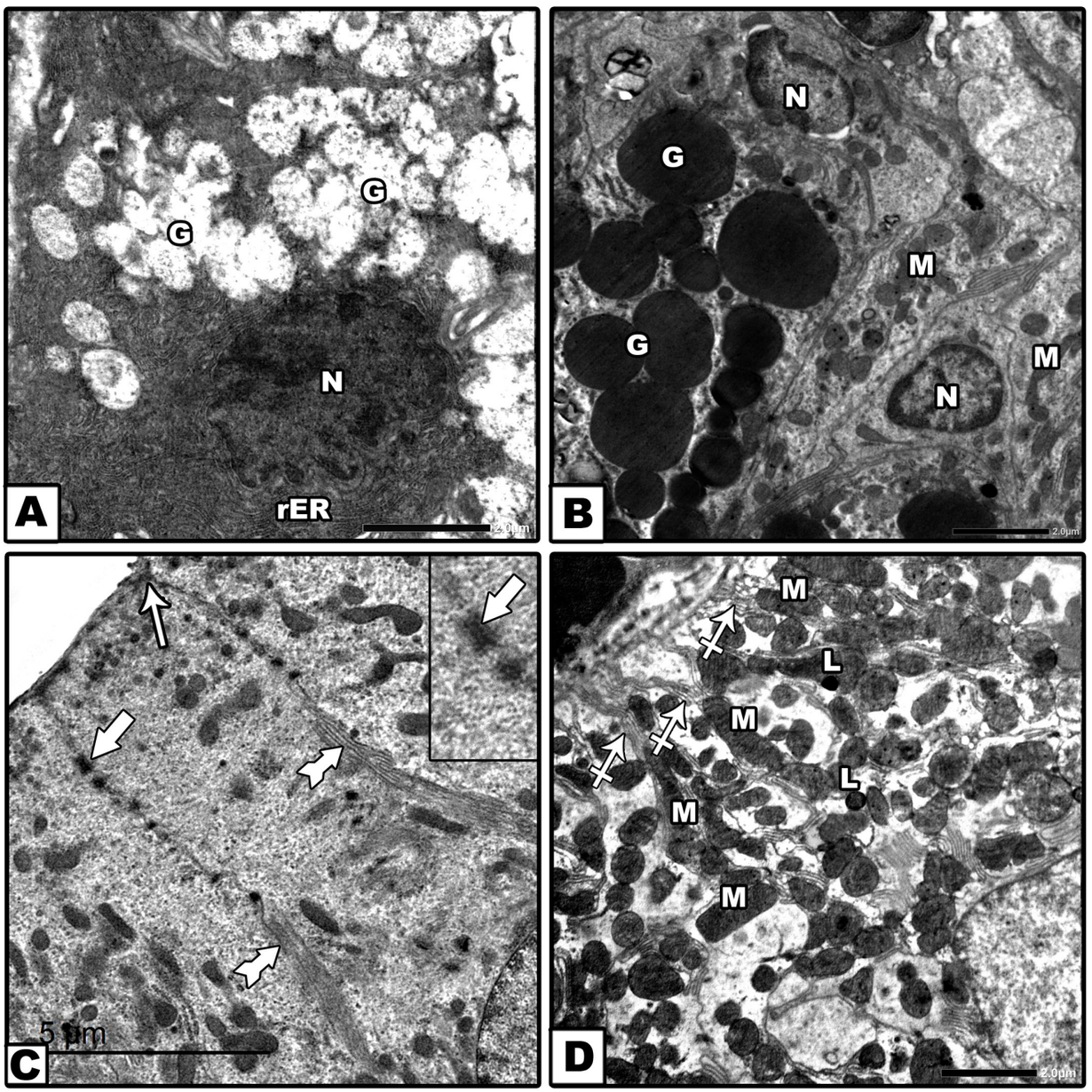

Fig. 14: Electron micrographs of the submandibular gland of Subgroup IVb. A: shows an acinar cell with apical numerous electron lucent granules (G) and packed parallel rER cisternae (rER). However, a heterochromatic nucleus with corrugated nuclear membrane (N) is seen. B: The cell of GCT reveals multiple electron dense granules (G), mitochondria (M). Heterochromatic nuclei (N) are noticed C: showing the striated duct with intact tight junction (arrow) and desmosomes between its cells (thick arrows). D: showing intact basal infoldings (crossed arrows) with irregular mitochondrial arrangement (M) and lysosomes (L) in the striated duct (Uranyl acetate & lead citrate; A, B &D X 4000; CX1500, Inset X3000).

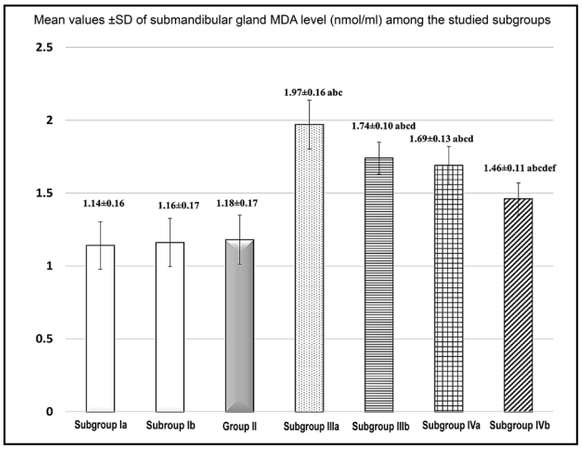

Histogram 1: Tissue MDA level (nmol/mL) among the studied subgroups. Data expressed as mean ± SD. $P \leq 0.05$ is significant. Test used: One way ANOVA followed by post-hoc tukey. A: significance vs subgroup Ia, B: significance vs subgroup Ib, C: significance vs subgroup II, D: significance vs subgroup IIIa, E: significance vs subgroup IIIb, F: significance vs subgroup IVa.

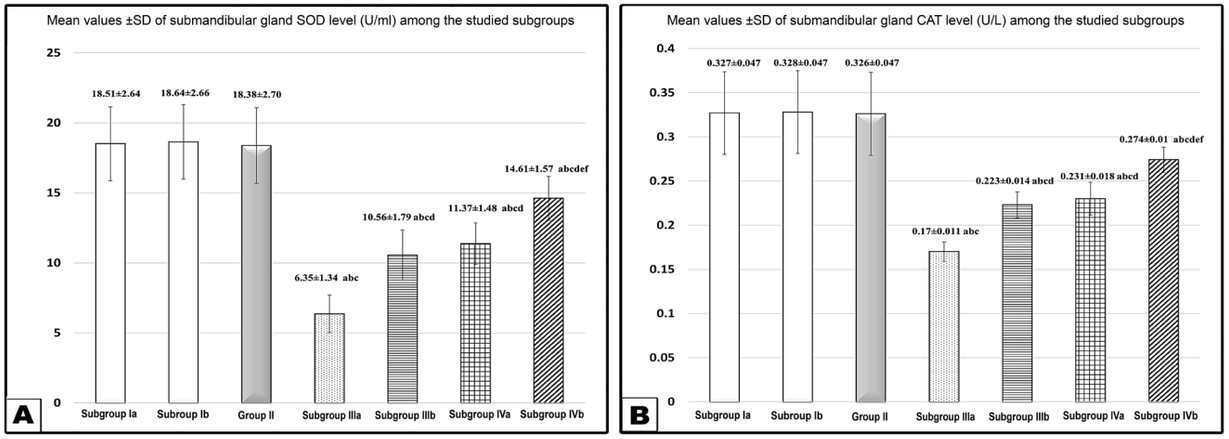

Histogram 2: Tissue SOD (U/mL) (A) and CAT (U/L) (B) activities among the studied subgroups. Data expressed as mean ± SD. $P \leq 0.05$ is significant. Test used: One way ANOVA followed by post-hoc tukey. A: significance vs subgroup Ia, B: significance vs subgroup Ib, C: significance vs subgroup II, D: significance vs subgroup IIIa, E: significance vs subgroup IIIb, F: significance vs subgroup IVa.

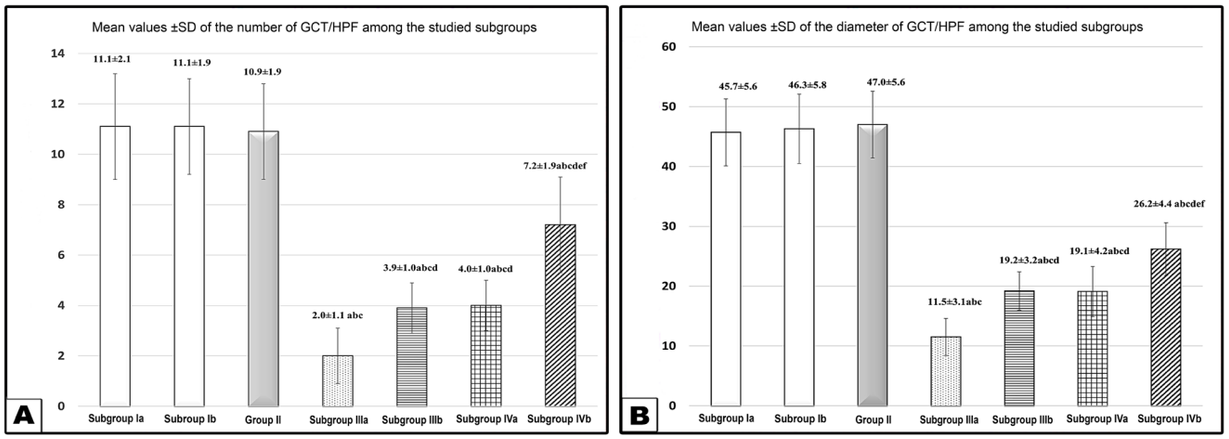

Histogram 3: The number (A) and diameter (nm) (B) of granular convoluted tubules / HPF among the studied subgroups. Data expressed as mean ± SD. $P \leq 0.05$ is significant. Test used: One way ANOVA followed by post-hoc tukey. A: significance vs subgroup Ia, B: significance vs subgroup Ib, C: significance vs subgroup II, D: significance vs subgroup IIIa, E: significance vs subgroup IIIb, F: significance vs subgroup IVa.

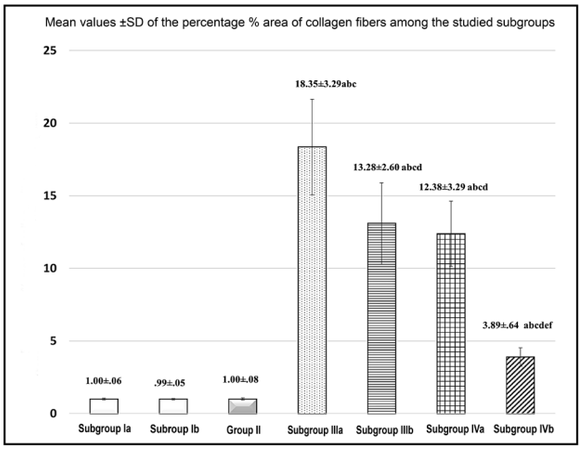

Histogram 4: Percentage % Area of collagen fibres among the studied subgroups. Data expressed as mean ± SD. $P \leq 0.05$ is significant. Test used: One way ANOVA followed by post-hoc Tukey. A: significance vs subgroup Ia, B: significance vs subgroup Ib, C: significance vs subgroup II, D: significance vs subgroup IIIa, E: significance vs subgroup IIIb, F: significance vs subgroup IVa.

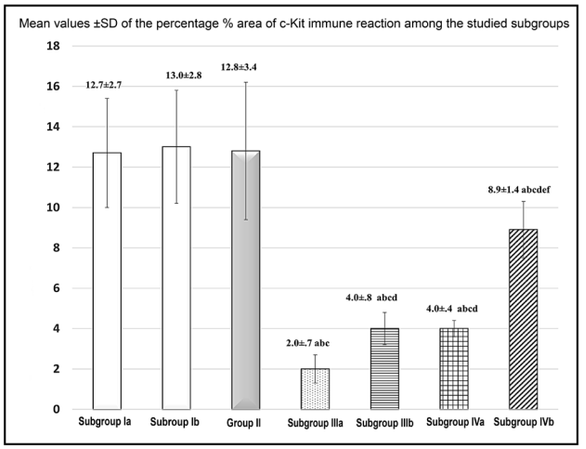

Histogram 5: Percentage % Area of c-Kit immune reaction among the studied subgroups. Data expressed as mean ± SD. $P \leq 0.05$ is significant. Test used: One way ANOVA followed by post-hoc tukey. A: significance vs subgroup Ia, B: significance vs subgroup Ib, C: significance vs Group II, D: significance vs subgroup IIIa, E: significance vs subgroup IIIb, F: significance vs subgroup IVa.

DISCUSSION

The present work was designed to assess the effect of hesperidin as an antioxidant to attenuate the changes provoked by two regimens of cisplatin in rat's submandibular gland, and its role in restoration of the glandular stem cells through biochemical, histological and immunohistochemical analysis.

The rodent submandibular gland differs from that of human in being composed of only one type of acini that is described as "atypical serous acini". It is like the serous acini in morphology and size, but its cytoplasm is paler than the serous acini and it secretes both amylase and mucin[33,34]. In our study, we demonstrated these atypical serous acini with their pyramidal lining cells that had basophilic cytoplasm and moderate electron dense or electro lucent granules by E/M. The Submandibular gland was considered an excellent choice in our study because it secretes vast amount of saliva (about 60%)[35] and the needed period for a drug to attain its highest concentration in the saliva was short when compared to the parotid saliva[20,36].

In Cisplatin treated subgroups, there were biochemical, histological and morphometric changes in the submandibular gland. The severity of these changes was dependent on the dose being more evident in subgroup IIIa that received the single high dose regimen compared to subgroup IVa that received multiple low dose regimen. This come in line with Astolfi *et al*.[37] who stated that the severity of the side effects is mainly influenced by the dosage of cisplatin and the higher initial dose produces a high concentration in tissues and a long excretion time. In many randomized trials, the cisplatin standard high dose schedule has been changed to weekly low dose regimen to avoid toxicity and to achieve good efficacy[38].

MDA is an outcome of free radicals induced peroxidation of lipids in the cells. So, It is widely used as oxidative stress marker[39]. SOD and CAT are antioxidant enzymes[40]. In the present study, the oxidant antioxidant ratio is affected; The tissue level of MDA showed significant elevation while the activities of SOD and CAT enzymes showed significant reduction in cisplatin groups compared to the control group especially subgroup IIIa. These data indicates that cisplatin can induce a state of oxidative stress. The same findings were documented by Zhu *et al*.[41].

In the current work, multiple cytoplasmic vacuolations were demonstrated in the cells of acini and ducts being marked in subgroup IIIa .Similar finding was reported with cisplatin administration by Hany *et al*.[42] and Dessoukey *et al*.[43]. The latter attributed this observation to the free radicals–induced damage of the cellular components. In addition, Shubin *et al*.[44] stated that the cytoplasmic vacuoles might be caused by the mitochondrial damage with subsequent failure of cell metabolism and sodium entrance that cause breakdown of large molecules and appearance of these vacuoles.

GCTs are considered a special duct in the submandibular gland of rodents located between the intercalated and striated ducts. They secrete regulatory peptides and nerve growth factors[45]. They showed degenerative changes with cisplatin treatment. Their lining cells were destructed leaving large empty spaces and showed loss of secretory granules. The present data were in line with Dessoukey *et al*.[43] who recorded such changes in the submandibular gland of animals receiving cisplatin. Furthermore, Elsharkawy and Alhazzazi[46] observed few eosinophilic granules in GCTs following antidepressant drugs. Krishnan *et al*.[47] mentioned that many factors contribute to the oxidative stress-induced ductal degeneration necrosis,

apoptosis, senescence, autophagy, calcium channels activation and damage of stem cells. Certain proteins and cytokines control these factors leading to cytotoxicity with subsequent ductal degeneration. Some nuclear changes were also detected in GCTs cells such as pyknosis or karyolysis. This might be due to the cisplatin-induced DNA damage directly or indirectly through the oxidative stress with the resulting cell death.

Statistical analysis revealed that the number and diameter of GCTs in subgroup IIIa and IVa was significantly lower than control group. But these parameters were significantly higher in subgroup IVa. In parallel with our finding Mahmouzadeh-Sagheb *et al*.[45] noticed reduced volume of granular convoluted tubules in the submandibular gland of lithium treated rats and they attributed this data to the suppression of cAMP-signaling pathway with subsequent reduction of DNA and protein synthesis in GCTs.

In the current work, dilatation of striated and interlobular ducts with stagnant secretion was noted in subgroups IIIa and IVa. Such finding was also noticed by Labah and Wahba[20] with cisplatin in the submandibular gland. Taghyan *et al*.[48] explained this ductal dilatation and the stagnant secretion by the mitochondrial damage with subsequent failure in transport process of secretions. Furthermore, Dessoukey *et al*.[43] mentioned that the damaging effect of cisplatin on the myoepithelial cells leading to stagnation of secretion in the duct lumen, failed saliva ejection and xerostomia.

In cisplatin treated animals, congested blood vessels were noticed. This finding could be due to the direct toxicity of cisplatin on the wall of the vessels that is followed by ischemia and congestion[49]. Moreover, the inflammation that aims to transport more blood to the inflamed degenerated tissue may be an additional cause[50,51]. Intraepithelial lymphocytes were also found. This was in accordance with Seyhan *et al*.[52] in the uterus of the rats receiving cisplatin. It might be as a result of excessive ROS and lipid peroxidation that damage the epithelial cell membranes followed by infiltration of lymphocytes[53].

Mallory's trichrome stained sections in the submandibular gland of subgroups IIIa and IVa showed excessive deposition of irregularly arranged collagen fibers in the thick capsule and septa, around the acini, ducts and blood vessels being more marked in subgroup IIIa. These results were proved by the significant elevation of the collagen fibers percentage area in such subgroups relative to control group I. However, the collagen fibers percentage area in subgroup IVa was significantly lower than subgroup IIIa. Same finding was recorded by Nakagawa *et al*.[54] in rat kidney after cisplatin administration. It was mentioned that the irregular collagen fibers is due to cisplatin- induced impaired collagen matrix formation[55]. Nishat and Kumar[56] proved that Parallel type I and perpendicular type III collagen fibers form a mesh-like structure that is histopathologically seen in the form of excessive fibrosis suggesting the role of type III collagen fibers in this process. Oxidative stress excites gene expression of collagen synthesis[57]. In addition Li *et al*.[58] declared cisplatin stimulates alpha1 chain of collagen type I through activation of its gene expression and disturb the extracellular matrix .

Regarding the c-kit immune staining in the current study, decreased immune reaction in the duct cells was observed in cisplatin treated subgroups IIIa and IVa and the percentage area of c-kit immune reaction in these subgroups showed significant decrease compared to control group I. Although, it revealed a significant increase in subgroup IVa relative to IIIa. This decrease could be due to depletion of stem cell pool. The present data were parallel with Lombaert *et al*.[59] and Jasmer *et al*.[60]. They noted, following irradiation; there was an evident decrease in the salivary gland stem cells and attributed the irreversible irradiation-induced hypo-salivation to the sterilization of these primitive glandular stem cells.

The current work revealed ultrastructural changes in the acinar and duct cells of cisplatin treated subgroups and supported the light microscopic findings. Similar data were provided by Labah and Wahba[20] and Dessoukey *et al*.[43] in the submandibular gland of cisplatin treated rats.

In this work, Fusion between secretory granules of the acinar cells was noted. In line with this finding Kassab and Tawfik[61] noticed merged secretory granules in the form of little lakes in the submandibular gland following caffeinated energy drink. These merged granules might indicate development of adaptive mechanisms[62] or might be due to oxidative stress caused by cisplatin with the resulting cellular damage and membranes decomposition[57]. Furthermore, cytoplasmic rarefaction was also observed in some duct cells. In agreement with this Nasr and Saleh[63] found such areas in renal cells of cisplatin –treated rats and referred this observation to the direct toxicity exerted by cisplatin

Cisplatin-induced damage of the cellular organelles was also demonstrated in this study. Dilated fragmented rER and dilated Golgi were found. In parallel with this result Abdel Mohsen *et al*.[64] noticed dilated Golgi in the Purkinje cells of cerebellum in cisplatin treated rats. These findings might be caused by the oxidative damage with subsequent peroxidation of lipids and injury to the cell and organelles membranes followed by sodium and water influx which in turn causes distention of these organelles[57,65]. Moreover, damaged, bizarre shaped, swollen mitochondria with cristolysis was found and might be due to cisplatin-induced toxicity and oxidative stress. Maj *et al*.[66] mentioned cisplatin causes accumulation of p53 in mitochondria followed by cell apoptosis and reduction in its membrane potential leading to malformed shape and cristae disorganization. In addition, mitochondria with variable length with electron density was reported by Nasr and Saleh[63] who attributed this to the mitochondrial response to overcome the stress of cisplatin on the renal

tissue. Secondary lysosomes were also frequently observed in the cells of ducts with cisplatin treatment in our work. It was mentioned that the amount and type of cytoplasmic lysosomes indicates the severity of cell damage[67].

The striated duct showed loss of basal infold¬ings in subgroups IIIa and IVa which might be a sign of cisplatin toxicity Similar finding was reported by Kassab and Tawfik[61]. Moreover, damaged the cell junctions was also found. It was documented that cisplatin causes delocalization and alterations in the junctional proteins[68].

In this study, pre-treatment with hesperidin in subgroups IIIb and IVb improved the biochemical, histological, and ultrastructural changes compared to subgroups IIIa and IVa. A significant reduction of MDA and significant elevation of SOD and CAT was found. The submandibular gland showed relatively intact structure however minimal focal changes were noticed. Moreover, the number and diameter of GCTs was significantly higher. These data indicate a good chemoprotection and antioxidant efficacy of hesperidin against cisplatin-induced submandibular damage. However, this improvement was less marked in subgroup IVa that received hesperidin and high single dose of cisplatin that might be explained by the severe oxidative stress which couldn't be prevented to a great extent by hesperidin.

Similarly, hesperidin has been used in series of previous studies and has shown to exert a chemoprotective effect in different tissues[17,18,20] or against other chemotherapeutic drugs[69-71] and a radioprotective effect in the submandibular gland[8] and various tissues[72]. In these studies, the hesperidin protective effect is through its actions against oxidative damage, inflammation, and apoptosis.

Mallory's trichrome stained sections of subgroups IIIb and IVb showed few regular collagenous fibers in the thin capsule, septa, periacinar and periductal and the percentage area of collagen fibers in these subgroups was significantly lower than subgroups IIIa and IVa respectively. It was previously mentioned that hesperidin can prevent hepatic fibrosis[73] and the experimentally induced pulmonary fibrosis[74]. The latter attributed the hesperidin antifibrotic effect to the reduction of oxidative injury and the molecular pathways that attenuate the modulation of inflammatory and pro-inflammatory cytokines to decrease deposition of collagen.

Strong and abundant c-Kit immune reaction in the cells of striated and intercalated ducts was found in subgroups IIIb and IVb and statistically proved by a significant increase of the percentage area of c-Kit immunoreactivity compared to subgroups IIIa and IVa. These findings could be due to antioxidant action of hesperidin allowing more stem cells to survive, proliferate thus restoring the glandular stem cell pool. In line with the present findings, Kwak *et al*.[75] mentioned there is an actively cycling stem cell population in the secretory complex of mouse submandibular gland. This complex comprises two parts; the acini and GCTs connected with the intercalated ducts together with the surrounding myoepithelial cells. They added, this population of progenitor stem cells mainly reside in special region in the intercalated ducts. They are found early in life and persists in adulthood contributing to the homeostasis, formation of ducts and may have effects in neoplasia or radiation-induced injury. In addition, Matias *et al*.[76] stated that the flavonoids can provide an alternative therapeutic approaches in the neural diseases therapy as they affect the function, survival and differentiation of neurons and Xiao *et al*.[77] mentioned that hesperidin can improve the self-renewal of mesenchymal stem cells and its ability for cartilage tissue repair through its powerful antioxidant activity.

CONCLUSION

Cisplatin causes dramatic alterations in the rat submandibular gland being more evident with the single high dose regimen than the multiple low dose regimen. Hesperidin exerts a powerful chemoprotective efficacy and alleviates cisplatin-induced submandibular damage through its antioxidant and antifibrotic activity. Moreover, hesperidin enhanced restoration of the stem cell population within the glandular secretory complex. So, hesperidin may have the potentiality for clinical use in cancer patients as it can be applied with cisplatin chemotherapy to prevent or reduce its side effects.

CONFLICT OF INTERESTS

There are no conflicts of interest.

REFERENCES

1. Petrović M, Todorović D. Biochemical and molecular mechanisms of action of cisplatin in cancer cells. Med Biol . 2016; 18(1): 12-18. UDC 615.277:[577.1+577.2.

2. Dasari S, Tchounwou P B. Cisplatin in cancer therapy: molecular mechanisms of action. Eur J Pharmacol. 2014; 740: 364-378. doi: 10.1016/j. ejphar.2014.07.025.

3. Zhou Y , Xu H , Xu W , Wang B , Wu H , Tao Y , Qian H. Exosomes released by human umbilical cord mesenchymal stem cells protect against cisplatin-induced renal oxidative stress and apoptosis in *vivo* and in *vitro*. Stem Cell Res Ther . 2013; 4(2): 34. doi: 10.1186/scrt194.

4. Elgamily M F , Denewar M. Potential benefit of Annona muricata extract in combating cisplatin induced injury of parotid gland in albino rats. Egypt Dent J . 2020; 66: 997-1007. doi: 10.21608/ edj.2020.23992.1027.

5. Aggarwal P , Hutcheson K A , Yu R , Wang J , Fuller C D , Garden A S. Genetic susceptibility to patient-reported xerostomia among long-term oropharyngeal cancer sur*vivo*rs. Sci Rep. 2022; 12(1): 1-12. doi: 10.1038/s41598-022-10538-9.

6. Ferraz C R , Carvalho T T , Manchope M F , Artero N A , Rasquel-Oliveira F S , Fattori V , Verri Jr W A. Therapeutic potential of flavonoids in pain and inflammation: mechanisms of action, pre-clinical and clinical data, and pharmaceutical development. Molecules. 2020; 25(3): 762. doi: 10.3390/ molecules25030762.

7. Stanisic D , Costa A F , Cruz G , Durán N, Tasic L. Applications of flavonoids, with an emphasis on hesperidin, as anticancer prodrugs: phytotherapy as an alternative to chemotherapy. Nat Prod Chem . 2018; 58: 161-212. doi:10.1016/B978-0-444-64056-7.00006-4.

8. Sakat M S , Kılıç K , Sahin A , Kiziltunc Ozmen H , Yıldırım S , Egilmez . The Protective Efficacy of Hesperidin and Thymol on Radiation-Induced Submandibular Gland Damage. The Laryngoscope; 2022:1-8. doi: 10.1002/lary.30405.

9. Salehinejad J , Mohtasham N , Bagherpour A , Abbaszadeh-Bidokhty H , Ghazi A. Evaluation of c-kit protein (CD117) expression in common salivary gland neoplasms. J oral maxillofac path . 2014: 18(2): 177. doi: 10.4103/0973-029X.140732.

10. Wang X , Qi S , Wang J , Xia D , Qin L , Zheng Z, Fan, Z . Spatial and temporal expression of c-Kit in the development of the murine submandibular gland. J M Histo . 2014: 45(4): 381-389. doi:10.1007/s10735-014-9570-7.

11. Wang W , Qi S , Wang J , Xia D , Qin L , Zheng Z, Fan Z . C-Kit, a double-edged sword in liver regeneration and diseases. Front Genet . 2021: 12: 598855. doi: 10.3389/fgene.2021.598855.

12. Lennartsson J, Rönnstrand L . Stem cell factor receptor/c-Kit: from basic science to clinical implications. Physio Rev . 2012; 92(4): 1619-1649. doi: 10.1152/physrev.00046.2011.

13. Nanduri L S , Maimets M , Pringle S A , Van Der Zwaag M , Van Os R P, Coppes R P. Regeneration of irradiated salivary glands with stem cell marker expressing cells. Radiother Oncol . 2011; 99(3): 367-372. doi: 10.1016/j.radonc.2011.05.085.

14. Aboraya D M , El Baz A , Risha E F , Abdelhamid F M. Hesperidin ameliorates cisplatin induced hepatotoxicity and attenuates oxidative damage, cell apoptosis, and inflammation in rats. Saudi J Biol Sci . 2022; 29: p. 3157-3166. doi: 10.1016/j. sjbs.2022.01.052.

15. Sahu B D , Kuncha M , Sindhura G J , Sistla R . Hesperidin attenuates cisplatin-induced acute renal injury by decreasing oxidative stress, inflammation and DNA damage. Phytomedicine. 2013; 20(5): 453-460. doi: 10.1016/j.phymed.2012.12.001.

16. Kamel K M , Abd El-Raouf O M , Metwally S A, Abd El-Latif H A , El-sayed M E . Hesperidin and rutin, antioxidant citrus flavonoids, attenuate cisplatin-induced nephrotoxicity in rats. J Biochem Mol Toxicol . 2014; 28(7): 312-319. doi: 10.1002/ jbt.21567.

17. Jia Y , Guo H , Cheng X , Zhang Y , Si M , Shi J , Ma D. Hesperidin protects against cisplatin-induced cardiotoxicity in mice by regulating the p62–Keap1–Nrf2 pathway. Food Funct . 2022; 13(7): 4205-4215. https://doi.org/10.1039/D2FO00298A.

18. Rezaeyan A , Fardid R , Haddadi G H, Takhshid, M A, Hosseinzadeh M , Najafi M , Salajegheh A . Evaluating radioprotective effect of hesperidin on acute radiation damage in the lung tissue of rats. J Biomed Phys Eng. 2016; 6 (3): 165. PMID:27853724

19. Esen E , Özdoğan F , Gürgen S G , Özel H E , Başer S , Genç S , Selçuk A . Ginkgo biloba and lycopene are effective on cisplatin induced ototoxicity? Journal Int Adv Otol . 2018; 14(1): 22. doi: 10.5152/ iao.2017.3137.

20. Labah D A , Wahba O M . Flaxseed oil: an emerging nutraceutical decimates cisplatin-induced submandibular salivary glands damage in rats. Tanta Dent J . 2017; 14(3): 105. doi:10.4103/tdj.tdj_7_17.

21. Dutton J W, Artwohl JE, Huang X, Fortman JD. Assessment of pain associated with the injection of sodium pentobarbital in laboratory mice (Mus musculus). J Am Assoc Lab Anim Sci. 2019; 1; 58 (3): 373-379. doi: 10.30802/AALAS-JAALAS-18-000094.

22. Tukozkan N , Erdamar H , Seven I. Measurment of total malondialdehyde in plasma and tissues by high-performance liquid chromatography and thiobarbitruric acid assay. Firat Tip Dergisi. 2006; 11(2): 88-92 .

23. Leite MF , De Lima AM , Sun Kang SJ, Santos MT, Otton R. Effect of astaxanthin and fish oil on enzymatic antioxidant system and α-amylase activity of salivary glands from rats. Braz J Oral Sci. 2014; 13(1): 58-63. doi:10.1590/1677-3225v13n1a12.

24. Aebi H: Catalase in *vitro*. In: Methods in enzymology. Academic Press. (1984) pp: 121-126. doi: 10.1016/ s0076-6879(84)05016-3.

25. Bancroft JD, Layton C: The hematoxlyin and eosin. In: Suvarna KS, Layton C, Bancroft JD (eds) Bancroft's theory and practice of histological techniques. 8th ed., Elsevier Health Sciences. China. (2018)pp: 126-138.

26. Kiernan JA: Histological and histochemical methods: theory and practice. 4th ed., Scion Publishing. Bloxham. (2015)pp: 571.

27. Nanduri L S , Lombaert I M , Van Der Zwaag M, Faber H , Brunsting J F , Van Os R P , Coppes R P. Salisphere derived c-Kit+ cell transplantation restores tissue homeostasis in irradiated salivary gland. Radiother Oncol . 2013; 108(3): 458-463. doi: 10.1016/j.radonc.2013.05.020.

28. Watanabe H , Takahashi H , Hata-Kawakami M , Tanaka A. Expression of c-kit and Cytokeratin 5 in the submandibular gland after release of long-term ligation of the main excretory duct in mice. Acta Histochem Cytochem. 2017; 50(3): 111-118. doi: 10.1267/ahc.17004.

29. Sanderson T, Wild G, Cull AM, Marston J, Zardin G: Immunohistochemical and immunofluorescent techniques. In: Suvarna KS, Layton C, Bancroft JD (eds) Bancroft's theory and practice of histological techniques. 8th ed., Elsevier Health Sciences. China. (2019) pp: 337-394.

30. Woods AE, Stirling JW: Transmission electron microscopy. In: Suvarna KS, Layton C, Bancroft JD (eds) Bancroft's theory and practice of histological techniques. 8th ed., Elsevier Health Sciences. China. (2019) pp: 434-476.

31. Manzato MC, de Santi F, da Silva AAS, Beltrame FL, Cerri PS, Sasso-Cerri E. Cimetidine-induced androgenic failure causes cell death and changes in actin, EGF and V-ATPase immunoexpression in rat submandibular glands. J Anat. 2021 ;239(1):136-150. doi: 10.1111/joa.13408.

32. Rosner B: Fundamentals of biostatistics. 8th ed., Cengage Learning. Boston. (2015) pp: 219.

33. Miclăuş V, Miclăuş V, Oana L, Ober C, Rus V, Pestean C. Observations concerning features of submandibular gland secretion in rats. Lucr. ştiinţ. med. vet. 2009;XLII(2): 382-386.

34. Parker GA, Picut CA: Atlas of histology of the juvenile rat. Academic Press. New York, London. (2016)pp: 175-177.

35. Hosoi K , Yao C , Hasegawa T, Yoshimura H , Akamatsu T. Dynamics of salivary gland AQP5 under normal and pathologic conditions. Int J Mol Sci . 2020; 21(4): 1182. doi: 10.3390/ijms21041182.

36. El Emam H F , Abd El Salam N N , Ghazy S E . IMPACT OF BONE MARROW STEM CELLS APPLICATION ON THE METHOTREXATE INDUCED SUBMANDIBULAR SALIVARY GLAND DEGENERATIVE CHANGES IN ALBINO RATS (HISTOLOGICAL AND IMMUNO-HISTOCHEMICAL STUDY). Egypt Dent J . 2019; 65: 1751-1762. doi: 10.21608/EDJ.2019.72931.

37. Astolfi L , Ghiselli S , Guaran V , Chicca M , Simoni E D I , Olivetto E , Martini A . Correlation of adverse effects of cisplatin administration in patients affected by solid tumours: A retrospective evaluation. Oncol Rep . 2013; 29 (4): 1285-1292. doi: 10.3892/or.2013.2279.

38. Szturz P , Wouters K, Kiyota N, Tahara M , Prabhash K, Noronha V , Vermorken J B . Low-dose vs. high-dose cisplatin: lessons learned from 59 chemoradiotherapy trials in head and neck cancer. Front Oncol . 2019; 9: 86. doi: 10.3389/fonc.2019.00086.

39. Ayala A , Muñoz M F , Argüelles S. Lipid peroxidation: production, metabolism, and signaling mechanisms of malondialdehyde and 4-hydroxy-2-nonenal. Oxid Med Cell Longev . 2014; 2014. doi: 10.1155/2014/360438.

40. Ighodaro O, Akinloye O. First line defence antioxidants-superoxide dismutase (SOD), catalase (CAT) and glutathione peroxidase (GPX): Their fundamental role in the entire antioxidant defence grid. Alexandria J Med. 2018; 54(4): 287-293. https://doi.org/10.1016/j.ajme.2017.09.001

41. Zhu K , Jiang L, Chu Y, Zhang Y S . Protective effect of selenium against cisplatin-induced nasopharyngeal cancer in male albino rats. Oncol lett . 2016; 12(6): 5068-5074. doi: 10.3892/ol.2016.5346.

42. Hany E , Sobh M A , Abou ElKhier M T , ElSabaa H M , Zaher A. R . The effect of different routes of injection of bone marrow mesenchymal stem cells on parotid glands of rats receiving cisplatin: a comparative study. Int J Stem Cells. 2017; 10 (2): 169. doi: 10.15283/ijsc17022.

43. Dessoukey S M , Halawa A M, Fathy I A, Kashkoush D M . The Effect of Adipose Derived Stem Cells versus Platelet Rich Plasma in Ameliorating Cisplatin-Induced Injury on The Submandibular Salivary Gland." A Comparative Histological Study". Egypt J Histol . 2021; 44(2): 406-417. doi: 10.21608/EJH.2020.32113.1309.

44. Shubin A V , Demidyuk I V, Komissarov A A , Rafieva L M , Kostrov S V . Cytoplasmic vacuolization in cell death and survival. Oncotarget.2016; 7: 55863. doi: 10.18632/oncotarget.10150.

45. Mahmouzadeh-Sagheb H R , Heidari Z , Noori Mugahi M. H .stereological study of the effects of lithium on morphology of submandibular gland. Pak. J. Biol. Sci. 2006; 9 (4): 746-49. doi:10.3923/pjbs.2006.746.749.

46. Elsharkawy G E Z , Alhazzazi T Y . The effect of the commonly used antidepressant drug amitriptyline (TCAs) on the salivary glands. J Dent Oral Disord Ther.2016; 4(4): 1-5. doi:10.15226/jdodt.2016.00163.

47. Krishnan M , Tennavan A , Saraswathy S , Sekhri T , Singh A K , Nair V . Acute Radiation-Induced Changes in Sprague-Dawley Rat Submandibular Glands: A Histomorphometric Analysis. World J Oncol .2017;8(2): 45. doi: 10.14740/wjon1021w.

48. Taghyan S A , Messiry H E , Zainy M A E . Evaluation of the toxic effect of silver nanoparticles and the possible protective effect of ascorbic acid on the parotid glands of albino rats: An in *vivo* study. Toxicol Ind Health . 2020; 36(6): 446-453. doi: 10.1177/0748233720933071.

49. Sánchez-González P D , López-Hernández F J , López-Novoa J M , Morales A I . An integrative view of the pathophysiological events leading to cisplatin nephrotoxicity. Crit Rev Toxicol . 2011. 41 (10): 803-821. doi: 10.3109/10408444.2011.602662.

50. El-Sakhawy M , Saeid S . Effect of long term administration of aspartame on the parotid salivary glands of male albino rats. Int J Adv Res. 2014; 2(3): 850-75.

51. Omar A I , Yousry M M , Farag E A . Therapeutic mechanisms of granulocyte-colony stimulating factor in methotrexate-induced parotid lesion in adult rats and possible role of telocytes: A histological study. Egypt J Histol . 2018; 41(1): 93-107. doi: 10.21608/EJH.2018.7525

52. Seyhan S , Sarıbaş G S , Akçay N C , Gurgen S G , Akyol S N , Göktaş G , Özoğul C . Investigation of the protective effects of acetyl l-carnitine on cisplatin-induced uterus toxicity. Gazi Medical Journal. 2018;29(4):294-298. doi:http://dx.doi.org/10.12996/gmj.2018.81

53. Rajendrakumar T , Rao S , Satyanarayana M L , Narayanaswamy H D , Byregowda S M . Effect of Andrographis paniculata on cisplatin induced renal histopathology in Wistar albino rats. Journal of Entomology and Zoology Studies.2020;8(3):589-596.

54. Nakagawa M , Karim M R , Izawa T , Kuwamura M , Yamate J . Immunophenotypical characterization of M1/M2 macrophages and lymphocytes in cisplatin-induced rat progressive renal fibrosis. Cells. 2021; 10(2): 257. doi: 10.3390/cells10020257.

55. Dantas M V M , Verzola M H A , Sanitá P V , Dovigo L N , Cerri P S , Gabrielli M A C . The influence of Cisplatin-based chemotherapy on the osseointegration of dental implants: An in *vivo* mechanical and histometrical study. Clin Oral Implants Res . 2019; 30(7): 603-616. doi: 10.1111/clr.13445.

56. Nishat R, Kumar H. Collagen fibers in oral submucous fibrosis - A polarizing microscopy study using two special stains. Comparative Study Indian J Pathol Microbiol. 2019; 62(4):537-543. doi: 10.4103/IJPM.IJPM_324_19.

57. Anan H, Gawish M F , Amer M G , Ibrahim N. E . Effects of low magnetic irradiation on morphology and ultrastructure of parotid glands in rats and amelioration by vitamin E. J Cytol Histol. 2012;3: 139. doi:10.4172/2157-7099.1000139.

58. Li S , Huang J, Guo Y, Wang J , Lu S , Wang B, Ulloa L . PAC1 Receptor Mediates Electroacupuncture-Induced Neuro and Immune Protection During Cisplatin Chemotherapy. Front Immunology. 2021; 12: 714244. doi: 10.3389/fimmu.2021.714244.

59. Lombaert I M , Brunsting J F , Wierenga P K , Faber H , Stokman M A , Kok T , Coppes R P . Rescue of salivary gland function after stem cell transplantation in irradiated glands. PloS one. 2008; 3(4): 2063. doi: 10.1371/journal.pone.0002063.

60. Jasmer K J , Gilman K E , Muñoz Forti K , Weisman G A , Limesand K H . Radiation-Induced Salivary Gland Dysfunction: Mechanisms, Therapeutics and Future Directions. J Clin Med. 2020;9(12): 4095. doi: 10.3390/jcm9124095.

61. Kassab A A , Tawfik S M . Effect of a caffeinated energy drink and its withdrawal on the submandibular salivary gland of adult male albino rats: A histological and immunohistochemical study. Egypt J Histo .2018; 41(1): 11-26. doi: 10.21608/EJH.2018.7518.

62. Abdeen A M , Essawy T , Mohammed S S . Effect of sofosbuvir administration and its withdrawal on the submandibular salivary gland of adult male albino rats: A histological and ultra-structural study. Open Access Maced J Medical Sci .2019;7(23): 4101. doi: 10.3889/oamjms.2019.868.

63. Nasr A Y , Saleh H A . Aged garlic extract protects against oxidative stress and renal changes in cisplatin-treated adult male rats. Cancer cell Int . 2014; 14(1): 1-12. doi: 10.1186/s12935-014-0092-x.

64. Abdel Mohsen A F , Ahmed N A W , Altaib Z M , Zaher S M. Effect of Cisplatin on Cerebellar Cortex of Albino Rat and Possible Protective Role of Granulocyte Colony Stimulating Factor versus Citrullus Lanatus Juice: A Histological Study. Egypt J Histo .2020; 43(3): 702-717. doi: 10.21608/EJH.2019.19193.1197.

65. Miller M A , Zachary J F. Mechanisms and morphology of cellular injury, adaptation, and death. Pathologic basis of veterinary disease.2017: 2–43. doi: 10.1016/B978-0-323-35775-3.00001-1.

66. Maj M A , Ma J , Krukowski K N , Kavelaars A , Heijnen C J . Inhibition of mitochondrial p53 accumulation by PFT-μ prevents cisplatin-induced peripheral neuropathy. Front Mol Neurosci . 2017: 10: 108. doi: 10.3389/fnmol.2017.00108.

67. Thurmond P , Yang J H , Li Y , Lerner L B , Azadzoi, K M . Structural modifications of the prostate in hypoxia, oxidative stress, and chronic ischemia. Korean Journal Urol . 2015; 56(3): 187-196. doi: 10.4111/kju.2015.56.3.187.

68. Zhang N , Cai J , Xu L , Wang H , Liu W. Cisplatin-induced stria vascularis damage is associated with inflammation and fibrosis. Neural Plast . 2020; 2020:1-13. doi: 10.1155/2020/8851525.

69. Patel P , Shah J . Protective effects of hesperidin through attenuation of Ki67 expression against DMBA-induced breast cancer in female rats. Life Sci. 2021; 285: 119957. doi: 10.1016/j.lfs.2021.119957.

70. Semis H S , Kandemir F M , Kaynar O , Dogan T, Arikan S M . The protective effects of hesperidin against paclitaxel-induced peripheral neuropathy in rats. Life Sci . 2021; 287: 120104. doi: 10.1016/j.lfs.2021.120104.

71. Gur C , Kandemir F M , Caglayan C , Satıcı E. Chemopreventive effects of hesperidin against paclitaxel-induced hepatotoxicity and nephrotoxicity via amendment of Nrf2/HO-1 and caspase-3/Bax/Bcl-2 signaling pathways. Chem Biol Interact . 2022; 365: 110073. doi: 10.1016/j.cbi.2022.110073.

72. Haddadi G H , Rezaeyan A , Mosleh-Shirazi M A , Hosseinzadeh M , Fardid R , Najafi M , Salajegheh A . Hesperidin as radioprotector against radiation-induced lung damage in rat: a histopathological study. J Med Phys . 2017; 42(1): 25. doi: 10.4103/jmp.JMP_119_16.

73. Morsy M A , Nair A B . Prevention of rat liver fibrosis by selective targeting of hepatic stellate cells using hesperidin carriers. Int J Pharm . 2018; 552(1-2): 241-250. doi: 10.1016/j.ijpharm.2018.10.003.

74. Zhou Z , Kandhare A D , Kandhare A A , Bodhankar S L . Hesperidin ameliorates bleomycin-induced experimental pulmonary fibrosis via inhibition of TGF-beta1/Smad3/AMPK and IkappaBalpha/NF-kappaB pathways. EXCLI J . 2019; 18: 723. doi: 10.17179/excli2019-1094.

75. Kwak M, Alston N, Ghazizadeh S. Identification of Stem Cells in the Secretory Complex of Salivary Glands. J Dent Res. 2016; 95(7):776-83. doi: 10.1177/0022034516634664.

76. Matias I , Buosi A S , Gomes F C A . Functions of flavonoids in the central nervous system: astrocytes as targets for natural compounds. Neurochem Inter . 2016; 95: 85-91. doi: 10.1016/j.neuint.2016.01.009.

77. Xiao S , Liu W , Bi J , Liu S , Zhao H , Gong N, Gong M , Anti-inflammatory effect of hesperidin enhances chondrogenesis of human mesenchymal stem cells for cartilage tissue repair. J Inflamm. 2018; 15(1): 1-8. doi: 10.1186/s12950-018-0190-y.

الملخص العربى

هيسبيريدين يخفف الخلل الناجم عن السيسبلاتين في الغدة تحت الفك السفلي للذكور البالغين من الجرذان البيضاء من خلال تنشيط الخلايا الجذعية فى المجموعة الافرازية (دراسة نسيجية وكيميائية مناعية وكيميائية حيوية)

علا عبد اللطيف يحيى[١]، سمر عادل عسكر[١،٢،٣]، وفاء سعد حامد[١]، نوال عوض حسنين[١]، و نهلة رضا سرحان[١]

قسم الأنسجة الطبية وبيولوجيا الخلية، كلية الطب، [١]جامعة المنصورة، [٢]جامعة السادس من أكتوبر، [٣]جامعة الدلتا

الخلفية: العلاج الكيميائي بالسيسبلاتين يستهدف العديد من الأورام. ومع ذلك ، فإنه يؤثر على الغدة تحت الفك السفلي مما يسبب قصورفي وظيفتها. هيسبيريدين له تأثيرات مضادة للأكسدة ومضادة للالتهابات.

الهدف من العمل: تقييم التغيرات البيوكيميائية والنسيجية الناتجة عن نظامين لتطبيق سيسبلاتين على الغدة تحت الفك السفلي للجرذان وتقييم تأثير الهسبريدين ضد هذه التغييرات.

المواد والطرق: تم تقسيم ٧٠ من ذكور الجرذان إلى ٤ مجموعات. المجموعة الأولى (الجرذان الظابطة) و المجموعة الثانية أعطيت هيسبيريدين (١٠٠ مجم / كجم / يوم) عن طريق الفم من اليوم الأول حتى نهاية التجربة. تلقت المجموعة الثالثة جرعة واحدة عالية من السيسبلاتين (عن طريق الحقن داخل الصفاق ١٢ مجم / كجم) في اليوم الثامن وتم تقسيمها إلى المجموعة الفرعية IIIa التي تلقت سيسبلاتين فقط وتلقى IIIb سيسبلاتين + هسبريدين كمجموعة II. تلقت المجموعة الرابعة جرعات منخفضة متعددة من السيسبلاتين (عن طريق الحقن داخل الصفاق ٦ مجم / كجم) مرة واحدة في الأسبوع بدءًا من اليوم الثامن وتنقسم إلى المجموعة الفرعية IVa التي تلقت سيسبلاتين فقط وتلقت IVb سيسبلاتين + هسبريدين كمجموعة II. تم استخراج الغدد تحت الفك السفلي ومعالجتها لإجراء دراسات كيميائية حيوية ونسيجية وكيميائية مناعية. تم استخدام c-Kit كعلامة للخلايا الجذعية.

النتائج: أظهرت المجموعات الفرعية IIIa و IVa تغيرات كيميائية حيوية ونسيجية وتغييرات في البنية التحتيةوالتى كانت أكثر وضوحًا في IIIa. كان هناك ارتفاع كبير في مالوندالديهايد وانخفاض فى أنشطة إنزيمات مضادات الأكسدة، واضطراب في بنية الغدة ، وتنكس فى الخلايا العنيبية وخلايا القنوات ، و زيادة ذات دلالةاحصائية في النسبة المئوية لمساحة ألياف الكولاجين وانخفاض ذو دلالةاحصائية في النسبة المئوية لمساحة رد الفعل المناعي c-Kit. أظهرت المجموعتان الفرعيتان IIIb و IVb تحسنًا في الصورة النسيجية للغدة مع زيادة ذو دلالة احصائية في النسبة المئوية لمساحة رد الفعل المناعي c-kit.

الخلاصة: يسبب السيسبلاتين تغيرات في الغدة تحت الفك السفلي تكون أكثر وضوحا بالجرعة العالية المفردة. يخفف هيسبيريدين جزئيًا هذه التغييرات من خلال تأثيره المضاد للأكسدة وتنشيط الخلايا الجذعية فى المجمع الافرازى. لذلك، يمكن استخدام الهسبريدين سريريًا مع العلاج الكيميائي لمنع آثاره الجانبية